Abstract

Austenitic twinning-induced plasticity (TWIP) steels, which rely on high manganese (Mn) contents, provide great potential in applications for structural components in the automotive industry. These steels exhibit an excellent combination of tensile strength and ductility, e.g. steels with tensile strengths above 1000MPa can present ductilities as high as 50%. These outstanding properties can be reached because the high manganese contents, characteristic of this steel grade, promote twinning as the main deformation mode.

The aim of this present work was to investigate the high temperature behavior, the static recrystallisation kinetics and the evolution of microstructure of high Mn steels when submitted to compression testing. In particular, the influence of homogenization heat treatment in the temperature range (950°C–1250°C) was studied and some observations were made regarding the evolution of plastic deformation at room temperature. Microstructures were examined using optical and scanning electron microscopes. Three TWIP steels with different compositions, i.e. 25%Mn, 20%Mn and 18%Mn, were examined and the results were used to evaluate the effect of the composition, as well as the processing route, on their behavior at high temperatures. In addition, double-hit tests and stress relaxation tests were performed on one grade of these TWIP steels.

Metallographic evaluations performed after tensile tests at room temperature revealed that the deformation mode of TWIP steels was twinning and that deformation twins were present since the first stages of deformation. Heat treatment parameters were carefully chosen to generate a new stress-free microstructure and, at the same time, limit the grain growth. 18%Mn and 25%Mn TWIP steels optimal temperature of heat treatment was 1100°C and it was of 1200°C for the 20%Mn TWIP steel. All the heat treatments were one hour long. A retarding effect of manganese on grain growth was detected.

Double-hit and stress relaxation tests performed on the 20%Mn TWIP steel were used to describe the softening behavior at high temperature of TWIP steels. The recrystallization kinetics was studied with stress relaxation tests and the influence of experimental parameters was evaluated. The result showed that static recrystallization in TWIP steels is little detectable by stress relaxation. However, metallographic observations revealed 100% recrystallization when the sample was tested at 950°C at a strain of 0.2. Both strain and temperature have little effect on recrystallization kinetics but seem to accelerate recrystallization when they are increased. Stress relaxation tests are very interesting from an experimental point of view because they imply a save of time and material; using the stress relaxation technique, a single test is necessary to draw a complete graph of recrystallized fraction as a function of time, whereas several tests would be necessary with double-hit testing.

Table of contents

1. Glossary

AHSS	Advanced High Strength Steels
Al	Aluminum
Ar	Argon
BH steels	Bake hardenable steels
C	carbon
°C	Celsius
C-Mn steels	Carbon-Manganese steels
CP steels	Complex Phase steels
CTM	Technological Centre of Manresa
DP steels	Dual Phase steels
DRX	Dynamic recrystallization
FB steels,	Ferritic-Bainitic steels
Fe	Iron
FCC	Face-centered cubic
HF steels	Hot-Formed steels
HSLA steels	High-Strength Low-Alloy steels
HSS	High Strength Steels
IF steels	Interstitial-free steels
IS steels	Isotropic steels
k, n	two constants characteristic of the kinetics in Avrami law
K	Kelvin
Mn	Manganese
MPa	MegaPascal = 10^9 Pascal
MS steels	Martensitic steels
OM	Optical microscope
Q_{def}	Activation energy for deformation
R	Gas constant R = 8.314 $Jmol^{-1}K^{-1}$
SEM	Scanning Electron Microscope
SFE	Stacking fault energy (
Si	Silicon
SRX	Static recrystallization

t	time
t_i	the interpass time
T	The temperature
T_N,	The Néel temperature
TRIP steels	Transformation-induced plasticity steels
TWIP steels	Twinning-induced plasticity steels
x_i	The molar fraction of element i
Z	Zener-Hollomon parameter
6012-1	18%Mn TWIP steel coming from Ottawa 1.5mm thick
6012-3-B,	18%Mn TWIP steel coming from Ottawa 4mm thick
6013-2	25%Mn TWIP steel coming from Ottawa 1.5mm thick
6013-4-B,	25%Mn TWIP steel coming from Ottawa 4mm thick
β	The magnetic moment
ε	strain, stretch
$\dot{\varepsilon}$, $\bar{\varepsilon}$	Strain rate
ε_c	Critical strain
ε_p	Peak strain
$\Delta G^{\gamma\to\varepsilon}$	The free molar enthalpy of the transformation $\gamma \to \varepsilon$
$\Delta G^{\gamma\to\varepsilon}_{FeMnX}$	Chemical contribution of all the elements in substitution in the FCC lattice
$\Delta G^{\gamma\to\varepsilon}_{mg}$	Magnetic term, due to the Néel transition (paramagnetic to antiferromagnetic)
μ_B	The Bohr magneton
ρ	The molar surface density of atoms in the {111} planes
σ or σ_0	tensile stress tension true stress
σ_M	Ultimate strength
$\sigma^{\gamma/\varepsilon} = 8\ \mathrm{mJ/m^2}$	The energy per surface unit of a {111} interface between γ and ε.
χ	Recrystallized fraction

2. Preface

2.1. Origin of the project

Cars, as any product, have to fulfill economical, ecological and legal requirements. Reducing fuel consumption, exhaust gases emission, and enhanced safety are the main objectives of the automotive industry nowadays. In this context, steel manufacturers had been developing new steel grades oriented to meet these goals. It has to be considered that any improvement on steel properties is of great interest because this material is present in many automobile components. Overall, the idea was to develop steel grades with higher strength levels so that the thickness of steel sheets could be decreased and, therefore the total weight of vehicles would be reduced. As a consequence, there would be a reduction of fuel consumption and exhaust gases emissions. The first development gave rise to a new generation of steels which relied on multiphase microstructures. This new generation of steels was called advanced high strength steels (AHSS) and it includes steels such as dual phase (DP) or transformation-induced plasticity (TRIP) steels. AHSS steels have a high strength level but still present a major drawback: every increase in strength represents a loss in ductility which means a poor formability and crash behavior.

This issue has been overcome by a new family of AHSS called twinning-induced plasticity (TWIP) steels. The main characteristic of TWIP steels is their excellent combination of strength and ductility which promotes a high energy absorption capability. These outstanding properties can be obtained with high contents in manganese which promotes twinning as the main deformation mechanism. These virtuous steels are the subject of this study.

2.2. Motivations

Many studies about TWIP steels have proved the great properties of this new steel grade but its deformation behavior at high temperature has not been extensively studied. It would be interesting to understand the deformation mechanism and see how the temperature affects the material while it is being hot rolled, for instance. The knowledge of the steel behavior during the deformation at high temperatures could be used to design deformation schedule aiming for an adequate microstructure in terms of grain size, without reaching excessive deformation loads. To achieve this goal, TWIP steels with different compositions were submitted to high temperature tests which were related to microstructure evaluations.

3. Introduction

3.1. Project objectives

This study about TWIP steels aim at achieving the general goal of a better understanding of the behavior at high temperature of high manganese content austenitic steel. This work is focused on the static recrystallization of TWIP steel, when submitted to high temperature deformations, and the influence of experimental parameters on recrystallization kinetics. These results are in the continuation of other projects, which dealt with static and dynamic recrystallization. The specific attention was turned to static and dynamic recrystallization because such phenomena occur during hot rolling of the steels. This stage of the manufacturing process determines the grain size and consequently the material properties. Mastering the behavior of TWIP steel is necessary to control the manufacturing process and obtain the desired properties.

In this study stress relaxation tests were performed at high temperature and metallographic evaluation of the tested samples were carried out to characterize static recrystallization of TWIP steels. A secondary objective of the project was to learn the experimental procedures for the preparation and the observation of metallographic samples, and also to learn how to analyze results and make conclusions.

3.2. Theoretical introduction

With the increasing cost of energy, automotive manufacturers aim at reducing gas consumption by decreasing vehicle mass, also for the benefit of the environment. Yet safety features should not be left aside. Meeting these goals requires steels with increased strength and improved formability. The steel industry responded by creating a new family of steels called advanced high strength steels (AHSS).

3.2.1. Definition of a TWIP steel

3.2.1.1. AHSS

Conventional high strength steels (HSS) and advanced high strength steels (AHSS) are presented on the following diagram extracted from *AHSS Application Guidelines, version 4.1, June 2009* (Fig. 3.1).

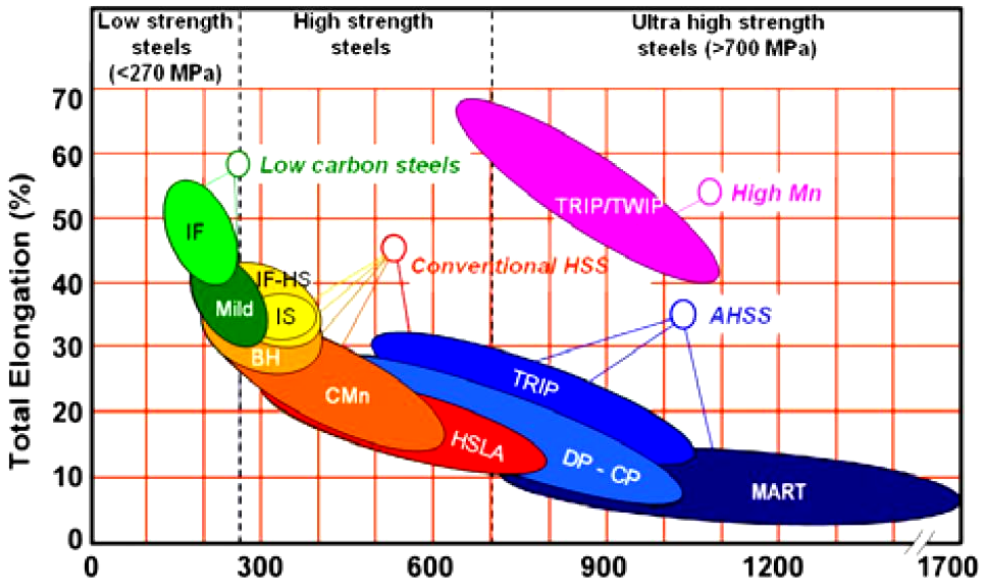

Fig. 3.1. Relationship between ultimate tensile strength and total elongation for various types of steels

Conventional HSS include Interstitial-free (IF) steels (Low strength and high strength), Mild steels, Isotropic (IS) steels, Bake hardenable (BH) steels, Carbon-Manganese (C-Mn) steels and High-Strength Low-Alloy (HSLA) steels. The common asset of this family is the single-phase ferritic microstructure. It is also commonly said that their yield strengths are between 210MPa and 550MPa and their tensile strengths are between 270MPa and 700MPa [WORLDAUTOSTEEL, 2009] .

The difference between AHSS and HSS is that AHSS microstructures contain other phases than ferrite or pearlite, i.e., martensite, austenite or bainite. During manufacturing, the cooling rate from the austenite or austenite plus ferrite phase is always controlled. This cooling rate control enables the steel manufacturers to predict the steel microstructure, which is of a great importance to be able to control its mechanical properties. AHSS usually present yield strengths higher than 550MPa, and tensile strength higher than 700MPa.

The higher strength presented by AHSS is often combined with a poorer ductility, as shown on the Fig. 3.1, which is the major drawback of these steels.

The AHSS family is composed of Dual Phase (DP) steels, Complex Phase (CP) steels, Martensitic (MS) steels and Transformation-Induced Plasticity (TRIP) steels, Ferritic-Bainitic (FB) steels, Hot-Formed (HF) steels and Twinning-Induced Plasticity (TWIP) steels as shown on Fig. 3.1.

Only TRIP and TWIP steels are going to be described since they are at stake in this report.

TRIP steel microstructure is made of retained austenite (minimum 5%) inside a matrix composed of ferrite, bainite and martensite present in different amounts (Fig. 3.2). Bainite and martensite confer to TRIP steels their strength. During deformation, TRIP steels strengthen due to two phenomena:

- The dispersion of hard second phases in soft ferrite creates a high work hardening;
- The retained austenite progressively transforms to martensite during deformation, which increases the work hardening rate at higher strain levels.

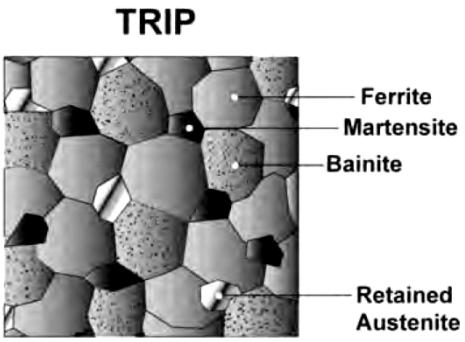

Fig. 3.2. TRIP steel microstructure

In high carbon TRIP steel, the retained austenite is more stable and transforms to martensite at high strain level. This last property makes TRIP steels very interesting to design car body elements that have to be resistant to crash since they have an excellent energy absorption capability [G. FROMMEYER, et al., 2003].

As it can be seen on Fig. 3.1, the main difference between TWIP steel and the other AHSS is the ductility.

This major difference is due to microstructure. TWIP steels are fully austenitic at room temperature which is possible thanks to a high content in manganese, between 15% and 30% (%wt). Austenite is a face-centered cubic structure which appears above 912°C for conventional steels, although it can be stable at room temperature for high Mn contents. Moreover high Mn contents are used in TWIP steels because manganese promotes twinning as deformation mode.

TWIP steels are normally composed of iron (Fe), 15% - 30% manganese (Mn), 1% - 3% silicon (Si) and 1% - 3% aluminum (Al). The main influence of Mn in TWIP steels is to control the stacking fault energy (SFE) and therefore the deformation mode (see paragraph 3.2.1.2). Aluminum is added to stabilize the austenite and it also strengthens the microstructure by solid solution hardening. Al also improves corrosion resistance. Silicon sustains the austenite transformation into martensite, since its lowers the SFE and increases the number of

stacking faults that are nucleation sites for martensite. It also strengthens austenite by solid solution hardening [CHARLES J, et al., 1982]. Carbon is an austenite stabilizer and strengthens the matrix by solid solution.

3.2.1.2. Deformation mechanism and SFE in TWIP steels

TWIP steels have an austenitic microstructure whose structure is face-centered cubic (FCC). This structure can be schematized as ABCABCABC (see Fig. 3.3). A stacking fault in a FCC crystal corresponds to a stacking which is locally of the type ABA. Thus, locally, a hexagonal structure (type ABABAB) is created within the FCC structure. This situation, even at a local scale, is energetically unfavorable.

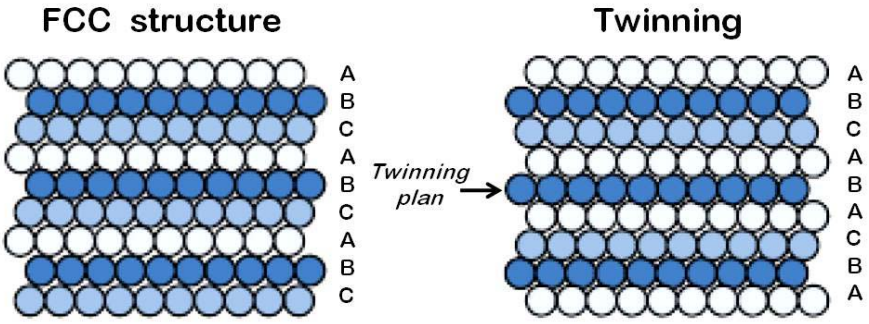

Fig. 3.3. Perfect crystal FCC compared to a twinning situation in a FCC structure

Stacking faults are normally generated in metals by dissociations of perfect dislocations. The energy necessary to create locally a hexagonal structure in a FCC structure is called the stacking-fault energy (SFE). The magnitude of the SFE controls the ease of cross-slip of dislocations in FCC metals [I. KARAMAN et al., 2002]. The SFE is primarily controlled by the temperature and the chemical composition and it determines the deformation modes, i.e., with a decreasing SFE, the deformation mechanisms are sequentially:

- Glide of dislocations in specific planes, which is the most common deformation pattern for metals.
- Formation of mechanical twins
- ε martensitic transformation (creation of a compact hexagonal phase)

Mechanical ε martensitic transformation only occurs if the SFE is below 18mJ.mol^{-1} and mechanical twinning occurs if the SFE is in the range of 12–35 mJ.mol^{-1} [S. ALLAIN, et al., 2004]. Other parameters such as grain size and shear modulus can influence the deformation mechanisms.

Therefore, FCC materials can be classified into three categories:

- FCC with middle and high SFE present the standard deformation mode; dislocation glide is planar at the beginning of the deformation and the deviated gliding is activated when the stress reaches a critical magnitude.
- Materials with small SFE exhibit dislocation glide occurring in planes and some twinning can be induced by deformation.
- For FCC microstructure with a very small SFE, dislocation glide is planar but twinning is no longer occurring. Instead, there is a phase transformation induced by deformation. This phenomenon corresponds to a transformation of austenite into ε martensite in the case of austenitic steels Fe-Mn-C [J.-L. COLLET, 2009]

Both slip and twinning are similar macroscopic shear mechanisms and both of them occur on a distinct plane and need a shear force to be activated. Deformation twinning is a very favorable mechanism, because it gives rise to a proper work hardening rate. The very fine twin lamellae can be regarded as extra intragranular obstacles that inhibit dislocation movement (comparable to grain refinement). This mechanism explains the great strength properties demonstrated by TWIP steels.

As reported in J.-L. Collet thesis, the deformation mechanism of low SFE can be described with three stages: simple planar gliding, multiple planar gliding and deformation-induced twinning. The first stage is characterized by an easy gliding of dislocations in a single plane. With increasing deformation, dislocation concentration raises and consequently the internal stresses too, which activate the second stage. Work hardening is very small during this first stage. Many gliding systems are activated during the second phase whose characteristic is a constant work hardening. After a certain critical stress, an intense twinning phenomenon is initiated, which is the beginning of the third phase. It is during this final stage that twinning occurs. Multiple twins are formed in the material which is the root of a high ductility and a major strength. These characteristics seem to be the result of the combination of dislocations gliding in slip planes and of deformation-induced twinning. The planar gliding activates the formation of stacking of dislocations which enables a constant and high work hardening when at least two gliding systems are activated.

3.2.1.3. TRIP / TWIP effect

As it was commented previously, SFE depends on the chemical composition and especially the manganese content when talking about austenitic Fe-Mn-C steel. H. Ding et al. studied two compositions of austenitic steels containing respectively 23.8%Mn and 33%Mn [H. DING, 2006], which have intermediate SFE. Their study revealed that the 23.8%Mn steel presented a TRIP and TWIP effect, while only TWIP effect was detected in the 33%Mn. This means that TRIP effect would be dominant in the deformation when the content of Mn is relatively low whereas only TWIP effect would appear when manganese content reaches a certain value. The effect on properties is that the steel showing combined effect of TRIP and TWIP has a high strength and a high plasticity and the steel whose deformation in dominated by the TWIP effect has a relatively high strength and an extraordinary plasticity.

The conclusions of this study were that TRIP effect may contribute on increasing the strength of the materials, while TWIP effect is beneficial to increase the plasticity of the materials (Fig. 3.4).

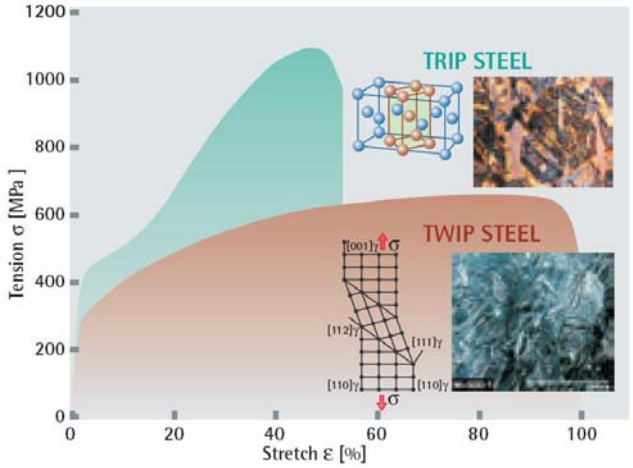

Fig. 3.4. Stress – strain diagram comparing TRIP steels to TWIP steels

3.2.2. Microstructure evolution during hot deformation

The stored energy due to the accumulated dislocations during deformation is generally lowered by three processes: recovery, recrystallization and grain growth. Annihilation and rearrangement of the dislocations occurs during recovery process. Recrystallization consists in the formation of new grains that are free of dislocation and the growth of them on the expense of the old deformed grains, leaving a new microstructure with low dislocation

density. The last step is grain growth, when the grains coarsen and the grain-boundary area is lowered. Recrystallization can take place during and after deformation; dynamic recrystallization occurs while deforming whereas after the deformation takes place static recrystallization.

The characteristic effect of work hardening, dynamic recovery and dynamic recrystallization on the stress-strain curve is illustrated in Fig. 3.5.

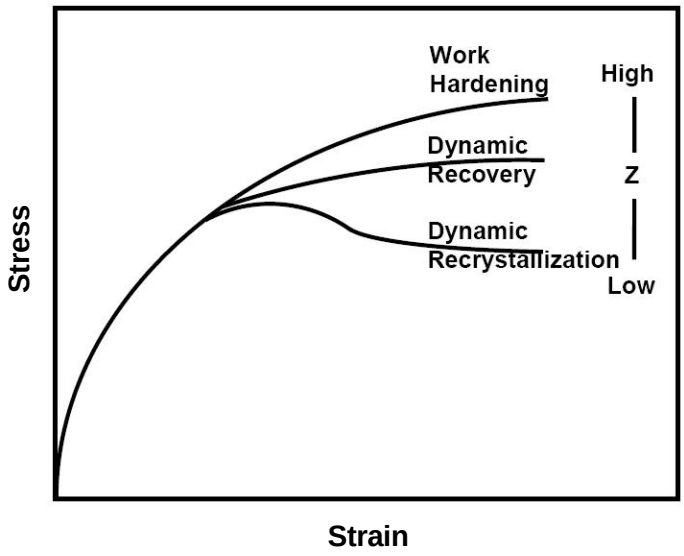

Fig. 3.5. Schematic illustration of work hardening, dynamic recovery and dynamic recrystallization during hot deformation

The flow curve is dependent on the conditions of deformation such as the temperature and the strain rate. The combined effect of these two variables is represented by the Zener-Hollomon parameter, Z (Eq. 3.1):

$$Z = \dot{\varepsilon}\exp\left(\frac{Q_{def}}{RT}\right) \quad (3.1)$$

where Q_{def} is the activation energy for deformation, $\dot{\varepsilon}$ is the strain rate and R is the gas constant (R = 8.314 J.mol^{-1}.K^{-1}).

3.2.2.1. Recovery

Recovery of the material is a process that occurs prior to recrystallization and is primarily due to changes in the dislocation structure. During recovery, the dislocations rearrange in configurations of lower energy.

Recovery is actually a series of events (see Fig. 3.6):

- formation of cells
- annihilation of dislocations within cells
- formation of low-angle subgrains
- subgrain growth

During subsequent recrystallization, these subgrains function as the nucleus of recrystallization.

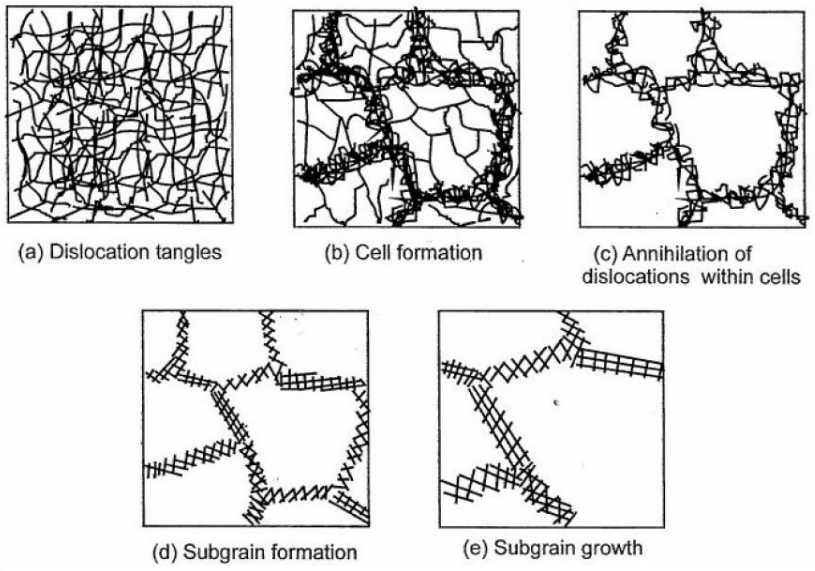

Fig. 3.6. Stages of recovery

3.2.2.2. Recrystallization

The definition of recrystallization according to Doherty et al. [R. D. DOHERTY et al., 1997] is "*the formation of a new grain structure in a deformed material by the formation and migration of high angle grain boundaries driven by the stored energy of deformation*". Consequently, recrystallization is the process which takes place when new dislocation-free grains are formed on the expense of the old deformed grains, leaving a new microstructure with low dislocation density.

The process is divided into nucleation of new grains and growth of them. In the nucleation process, the subgrains must have an energy advantage - a larger size - to be able to grow, rather than shrink and vanish. Hence, for the recrystallization to take place, a critical subgrain size has to be reached. Preferable nucleation sites for recrystallization are grain boundaries,

but when the grains are very large, intragranular nucleation, occurs as well [LINDA LISSEL, Thesis, Sep. 2006].

The recrystallized grain size is reduced by large deformations which introduce smaller subgrains and thereby increases the number of nucleation sites for recrystallization. There is also a strong temperature dependence on the recrystallized grain size. At lower temperature, finer recrystallized grains are obtained due to the lower mobility of recrystallizing grain boundaries and consequently slower growth rate of new grains [W. P. SUN et al., 1996]. The slower growth rate promotes additional nucleation during recrystallization which consequently gives finer recrystallized gains. As the initial grain size is decreased, this effect becomes less significant.

The nucleation and growth of recrystallized grains give a sigmoid shape of recrystallization kinetics curve which represents the recrystallized fraction as a function of log(time). Typical recrystallization curves are illustrated in Fig. 3.7. Recrystallization is a thermally activated process and the temperature dependence for static recrystallization is illustrated in Fig. 3.7 for a C-Mn steel.

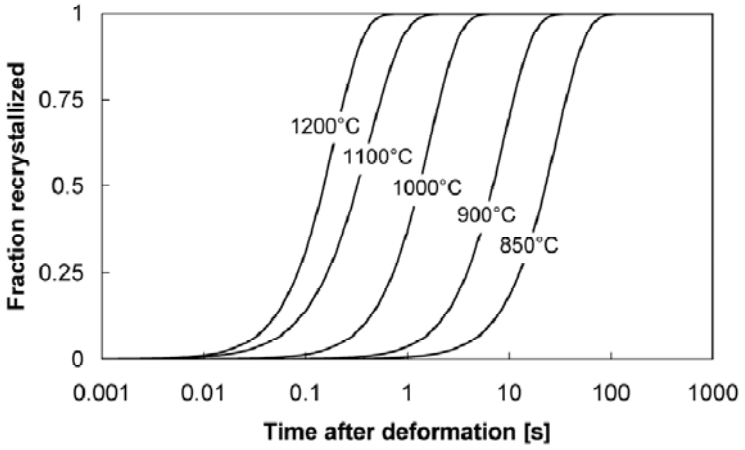

Fig. 3.7. Example of recrystallization curves for a plain C-Mn steel pre-strained to 0.2 at a strain rate of 1 s^{-1} deformed and annealed at 850°C-1200°C

Dynamic recrystallization (DRX)

If dynamic recrystallization occurs, the flow-stress raises to a peak value followed by a lower steady-state flow-stress, as shown on Fig. 3.5. Dynamic recrystallization is promoted by low strain rates and high temperature. If the strain rate is low enough the flow stress does not reach a steady-state flow-stress after the peak, but oscillates around a certain value due to successive cycles of recrystallization occurring concurrently with the deformation. At higher strain rates there is a single peak behavior of dynamic recrystallization (Fig. 3.8).

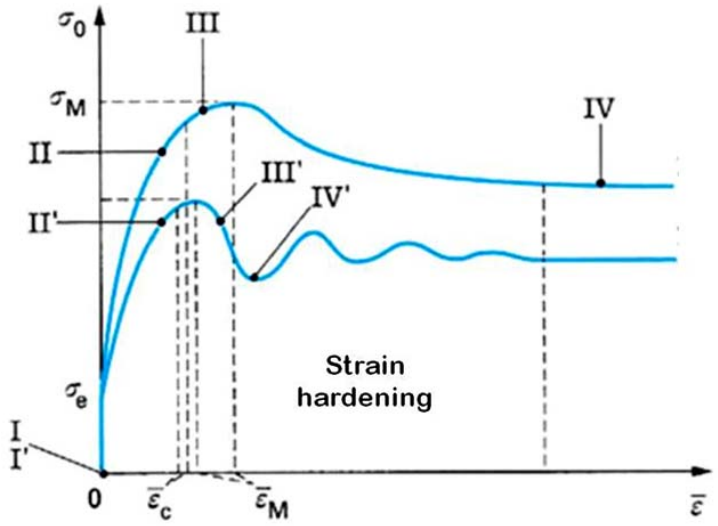

Fig. 3.8. Schematic representation of single-peak and multiple-peak dynamic recrystallization (Roman numbers refer to fig 3.9)

What differs between these two dynamic recrystallization modes is the mechanism of nucleation. In the single peak case, nucleation essentially occurs along existing grain boundaries. The growth of each grain is stopped by the concurrent deformation. In the multiple peak case, the growth of each new grain is terminated by boundary impingement and not by the concurrent deformation [J. G. LENARD, 1999].

For dynamic recrystallization to take place, a critical strain has to be reached. Some low fraction of recrystallization takes place before reaching the maximum flow stress at the peak strain . Hence, the peak strain in the stress-strain curve is always greater than the critical strain required to initiate dynamic recrystallization.

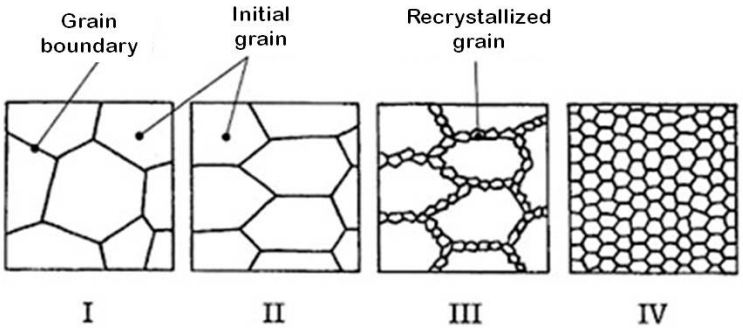

Fig. 3.9. Microstructure evolution during dynamic recrystallisation

Static recrystallization (SRX)

Static recrystallization occurs after a deformation below the critical strain and follows the two common stages of recrystallization a certain time after deformation has been applied: nucleation and growth of new grains. Full recrystallization occurs when work hardened grains have been fully replaced by equiaxed grains. Static recrystallization depends on time since it occurs after deforming the material. Its kinetics can be simulated by an Avrami law (Eq. 3.2):

$$X = 1 - \exp\left(kt^n\right) \tag{3.2}$$

Where χ is the recrystallized fraction, t is the time and k and n are two constants characteristic of the kinetics. Static recrystallization requires an incubation time to renew the microstructure. The main parameters that govern the static recrystallization are temperature, strain and strain rate.

When a high strain is applied on the material, a lot of energy is stored inside the microstructure so the static recrystallization kinetics is accelerated for nucleation and growth of new grains. Therefore, at high strain, more grains are nucleated and the final grain size is smaller. When the temperature is high, the work hardening at the end of the deformation is low and so there are fewer germination sites and the resulting grain size is larger. Also, a high temperature increases the kinetics of grain growth. Therefore, the temperature tends to accelerate the static recrystallization kinetics. The impact of strain rate on static recrystallization kinetics is smaller than the other parameters. Nevertheless, a higher strain rate implies faster kinetics. This phenomenon is the consequence of a greater work hardening [P. FABRÈGUE].

3.2.2.3. Grain growth

The recrystallization is completed when a new microstructure free of dislocations has been generated throughout the whole material. At this stage of the homogenizing process, the steel has a new grain size which is the minimum possible for a certain composition and the amount of accumulated strain and the temperature influence this new grain size. Most of the internal energy has been dissipated but the remaining energy can be dissipated by the mechanism of grain growth. This phenomenon is driven by the decrease in energy per unit volume which is accomplished by the reduction of grain boundary area and by the increase of average grain boundary curvature. The result is an increasing grain size [J.M. CABRERA MARRERO, 1995]

3.2.3. Experimental methods to determine SRX

3.2.3.1. Double-hit test

To measure the recrystallization kinetics, double-hit tests were performed. The shape of the curve showed in the Fig. 3.10 is obtained after such tests for austenitic steels.

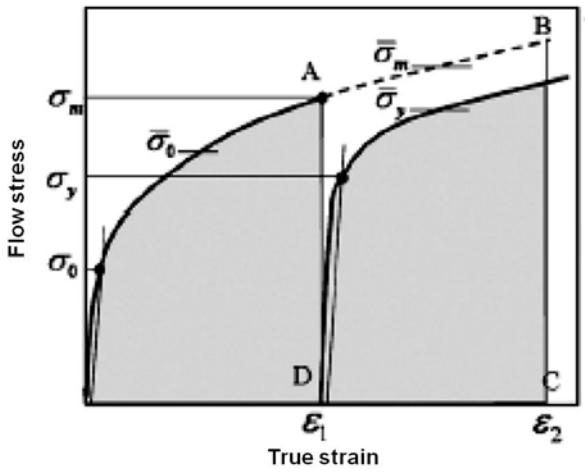

Fig. 3.10. Flow stress vs. true strain curve for a double-hit test

This curves is used to calculate the recrystallized fraction at a given strain rate, temperature and interpass time. The strain applied during the first deformation determines the recrystallization kinetics during the interpass time. During the first deformation, it can be observed a linear increase of the stress up to the magnitude of σ_0, which corresponds to the elastic limit. Then the stress reaches a maximum value for this first deformation, called σ_m, which is the stress for the corresponding strain ε_1. After this first deformation, the load is released during a certain time called the interpass time. At the end of this time, the load is again applied to reach the strain ε_2 [P. D. HODGSON, et al., 2004].

If no static recrystallization was occurring, the elastic limit of the second deformation, σ_y, should be equal to σ_m. Nevertheless, when static recrystallization occurs, σ_y is smaller than σ_m. Therefore, after this double-hit test, the recrystallized fraction is calculated with the following formula (Eq. 3.3):

$$\chi = \frac{\sigma_m - \sigma_y}{\sigma_m - \sigma_0} \times 100 \qquad (3.3)$$

There are different ways to calculate σ_0, σ_y and σ_m

- The tangent method: it is processed directly on the graph. Two tangents are drawn on the corresponding deformations and the chosen value is the value of the last common point between the curve and the tangent.
- The 0.2% method: a line is drawn parallel to the linear increase of the deformation for the two passes. The first one is adjusted to cross the axis at zero. Then the values at 0.2% are selected to determine the parameters. This method is often preferred because it is more precise and reproducible [K.P. RAO, et al., 1998]

When the recrystallized fraction is represented vs. the interpass time, the curve obtained has a sigmoid shape, as shown in the Fig. 3.7 (when the temperature, the strain rate and the strain at the first deformation are kept constant).

3.2.3.2. Stress relaxation test

Stress relaxation test is another method to determine softening behavior of steels. The test can be split into two stages. The first stage is a simple compression stage at a given temperature. When the selected strain is reached, the second stage begins. This second part of the test consist in keeping the strain constant, at the same temperature, and the decrease in stress is monitored as a function of time. The decrease in stress, which is due to rearrangements in the material, is recorded during a sufficient time for the steel to fully relax internal stresses.

Stress relaxation tests have extensively been used to characterize precipitation during hot deformation. Precipitation is a phenomenon that strengthens the material and promotes a slower decrease in the slope of the diagram stress vs. time. Quite the reverse, recrystallization is a phenomenon that softens the material so it is seen in the diagram stress vs. time by a higher decrease in stress relaxation, as illustrated in Fig. 3.11.

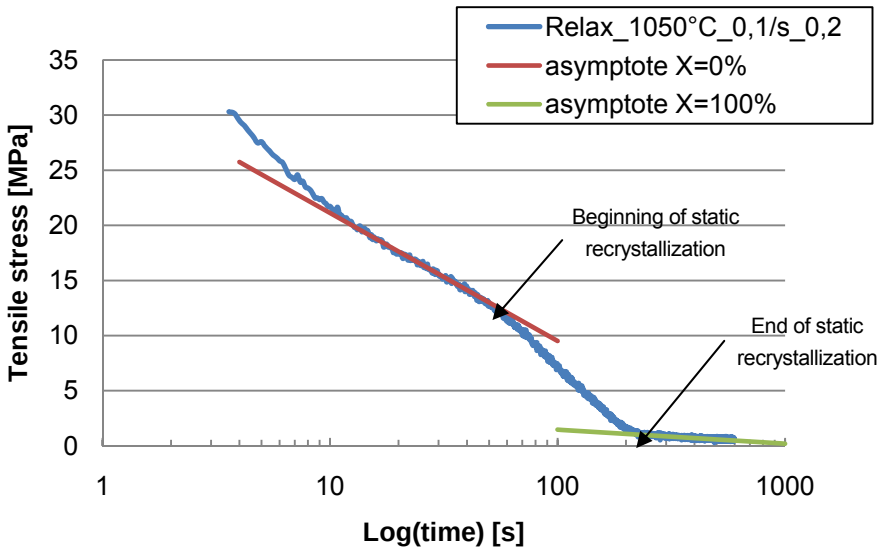

Fig. 3.11. Example of a stress relaxation curve revealing static recrystallization

A model has been developed to calculate the recrystallized fraction using stress relaxation curves [L.P. Karjalainen, 1995]. It considers that the first part and the third part of the curve can be described by straight lines having the following equation (Eq. 3.4):

$$\sigma = \sigma_0 - \alpha \log t \tag{3.4}$$

where σ is the true stress, t is the relaxation time and σ_0 and α are constants. Then it is assumed that the first linear part corresponds to stress relaxation in the strained austenite by the creep process. As for the third part, also linear, it is considered to be the stress relaxation of the soft austenite. It must be ensured that this last stage correspond to the fully softened material which refers to a fully recrystallized material. The rapid change in stress level between these two stages is due to static recrystallization of work hardened austenite. Then the stress level in the softening stage is expressed in terms of the relative fraction of the two phases, work hardened and fully softened, by a rule of mixture (Eq. 3.5).

$$\sigma = (1-\chi)(\sigma_1 - \alpha_1 \log t) + \chi(\sigma_2 - \alpha_2 \log t) \tag{3.5}$$

χ refers to the recrystallized fraction. 1 and 2 refer to the first stage (work hardened) and the third stage (soft material) of the stress relaxation curve respectively. From this equation χ can be calculated as follows (Eq. 3.6):

$$\chi = \frac{(\sigma_1 - \alpha_1 \log t) - \sigma}{(\sigma_1 - \sigma_2) - (\alpha_1 - \alpha_2) \log t} \tag{3.6}$$

4. Material and methods

4.1. Material properties

4.1.1. Chemical composition

For this work, three TWIP steels were studied. Their compositions are shown in the following table (Table D.1).

TWIP steel variety	%Mn	%C	%Si	%Al	%Fe
TWIP 18%Mn	18	0.55	0.8	-	Balance
TWIP 20%Mn	20	0.44	1.50 – 1.84	1.46	Balance
TWIP 25%Mn	25	0.03	1.8	-	Balance

Table D.1. Chemical compositions of the three TWIP steel

4.1.2. Stacking fault energy (SFE)

4.1.2.1. SFE calculation

All the information to calculate the stacking fault energy was extracted from an article written by A. Dumay, et al. [A. DUMAY et al., 2008]

In FCC structures, twinning is due to stacking faults extending in parallel adjacent dense planes. Extending them every two planes leads to the formation of ε martensite. A stacking fault can be modeled by two atomic layers of ε martensite within the dense planes. This leads to the equation 4.1 for the calculation of the SFE:

$$\Gamma = 2\rho\Delta G^{\gamma\rightarrow\varepsilon} + 2\sigma^{\gamma/\varepsilon} \quad (4.1)$$

with $\Delta G^{\gamma\to\varepsilon}$ the free molar enthalpy of the transformation $\gamma \to \varepsilon$, ρ the molar surface density of atoms in the {111} planes and $\sigma^{\gamma/\varepsilon} = 8\mathrm{mJ/m^2}$, the energy per surface unit of a {111} interface between γ and ε.

According to the simplified previous model for the Fe–Mn–C system, the free molar enthalpy of martensite formation can be written as follows (Eq. 4.2):

$$\Delta G^{\gamma\to\varepsilon} = \Delta G^{\gamma\to\varepsilon}_{FeMnX} + x_c \Delta G^{\gamma\to\varepsilon}_{FeMnX/C} + \Delta G^{\gamma\to\varepsilon}_{mg} \quad (4.2)$$

Using the regular and subregular solution model, $\Delta G^{\gamma\to\varepsilon}_{\mathrm{FeMnX}}$ is the chemical contribution of all the elements in substitution in the FCC lattice (Eq. 4.3). The Fe–Mn excess term is taken into account but the others involving the addition elements are neglected because of the little quantities considered, except for silicon:

- $\Delta G^{\gamma\to\varepsilon}_{FeMnX} = \sum_i x_i \Delta G^{\gamma\to\varepsilon}_i + x_{Fe}x_{Mn}[C + D(x_{Fe} - x_{Mn})] + x_{Fe}x_{Si}[E + F(x_{Fe} - x_{Si})]$

$$\Delta G^{\gamma\to\varepsilon}_i = A_i + B_i T \qquad i = Fe, Mn, Si \quad (4.3)$$

with x_i the molar fraction of element i, T the temperature and {Ai}, {Bi}, C, D, E and F fitting parameters.

An empirical law has been improved (Eq. 4.4), to account for an increasing carbon effect with manganese content:

- $\Delta G^{\gamma\to\varepsilon}_{\mathrm{FeMnX/C}} = \frac{a}{x_c}\left(1 - e^{-bx_c}\right) + cx_{\mathrm{Mn}}$ (4.4)

where a, b and c are fitting parameters.

$\Delta G^{\gamma\to\varepsilon}_{\mathrm{mg}}$ is a magnetic term, due to the Néel transition (paramagnetic to antiferromagnetic) of each phase φ (Eq. 4.5):

- $\Delta G^{\gamma\to\varepsilon}_{mg} = G^{\varepsilon}_m - G^{\gamma}_m$ (4.5)

Where $G^{\varphi}_m = RT \ln\left(\frac{\beta^{\varphi}}{\mu_B} + 1\right) f(\tau)$ $\varphi = \gamma, \varepsilon$ and $\tau = \frac{T}{T^{\varphi}_N}$,

with β^{φ} and T^{φ}_N, respectively, the magnetic moment and Néel temperature of phase φ, μ_B the Bohr magneton and f a polynomial function which was formulated in an article written by LIN LI X [LIN LI X et al., 1997] (Eq. 4.6 and 4.7).

When $\tau \leq 1$:

$$f(\tau) = 1 - \left\{\frac{79\tau^{-1}}{140p} + \frac{474}{497}\left[\frac{1}{p} - 1\right]\left[\frac{\tau^3}{6} + \frac{\tau^9}{135} + \frac{\tau^{15}}{600}\right]\right\}/D \quad (4.6)$$

And when $\tau > 1$

$$f(\tau) = -\left[\frac{\tau^{-5}}{10} + \frac{\tau^{-15}}{315} + \frac{\tau^{-25}}{1500}\right]/D \quad (4.7)$$

With $p = 0.28$ and $D = 2.342456517$

All the parameters used for the calculation of the SFE are in the following table (Table D.2)

ρ	2.94×10^{-5} mol.m^{-2}
$\sigma^{\gamma/\varepsilon}$	8 mJ.m^{-2}
$\Delta G_{Fe}^{\gamma\to\varepsilon}$	$-2243.38 + 4.309$T J.mol^{-1}
$\Delta G_{Mn}^{\gamma\to\varepsilon}$	$-1000.00 + 1.123$T J.mol^{-1}
$\Delta G_{Si}^{\gamma\to\varepsilon}$	$-560-8$T J.mol^{-1}
$\Delta G_{FeMn}^{\gamma\to\varepsilon}$	C$= 2873$ J.mol^{-1}; D$=-717$ J.mol^{-1}
$\Delta G_{FeSi}^{\gamma\to\varepsilon}$	E$= 2850$ J.mol^{-1}; F$= 3520$ J.mol^{-1}
$\Delta G_{FeMnX/C}^{\gamma\to\varepsilon}$	a$= 1246$ J.mol^{-1}; b$= 24.29$ J.mol^{-1}; c$=-17{,}175$ J.mol^{-1}
$\frac{\beta^{\varepsilon}}{\mu_B}$	$0.62x_{Mn} - 4x_C$
$\frac{\beta^{\gamma}}{\mu_B}$	$0.7x_{Fe} + 0.62x_{Mn} - 0.64x_{Fe}x_{Mn} - 4x_C$
T_N^{ε}	$580x_{Mn}$
T_N^{γ}	$250\ln(x_{Mn}) - 4750x_Cx_{Mn} - 13x_{Si} + 720$
R	8.31 J.mol^{-1}.K^{-1}

Table D.2. Parameters for the calculation of the SFE

4.1.2.2. SFE for TWIP steels

The stacking fault energy has been calculated for each TWIP steels, at a temperature of 20°C (293K). They are presented in the following table (Table D.3).

TWIP steel variety	Stacking fault energy $mJ.m^2$
18%Mn TWIP	19.58
20%Mn TWIP	18.58
25%Mn TWIP	12.33

Table D.3. Stacking fault energy of 3 TWIP steels

According to S. Allain, [S. ALLAIN, et al., 2004] these values are in the range of SFE which promote twinning as the deformation mechanism. Therefore, from the point of view of the SFE, it can be assumed that the steels are TWIP steels.

4.2. Manufacturing process of the TWIP steels

The three compositions of TWIP steel, which will be compared in this work, were not manufactured in the same Institute.

20%Mn steel: This steel was produced in The Metallurgical Research Institute in the University Michoacana of San Nicolás de Hidalgo, Morelia Michoacán, Mexico by melting and casting from an open induction furnace of 25kg. Using this process, rectangular bars of 62mm x 75mm were obtained, with a length of approximately 250mm. From theses ingots 60mm long pieces were cut. Each piece was subjected to a reheating treatment at 1200°C for 2 hours prior to hot rolling to obtain 13mm thick plates.

18%Mn and 25%Mn steels: These two TWIP steels were produced in the CANMET Materials Technology Laboratory, in Ottawa, Ontario, Canada. The ingots obtained after casting were hot rolled to obtain a thickness of 4 mm (Fig. 4.1) and then coiled at a temperature of 650ºC. (It was proved in a prior study done in the LMT-CANMET that this temperature gives

Fig. 4.1. Plate of 18% TWIP steel of 4mm thick

the most interesting properties to the steels.)

4.3. Homogenization heat treatment

The homogenization heat treatments were performed in a high temperature tubular furnace *Hobersal ST-16* under controlled atmosphere (Ar). Austenitic steels oxidize very quickly at high temperature so it is compulsory to protect the material from corrosion with inert gas (see Fig. 4.2)

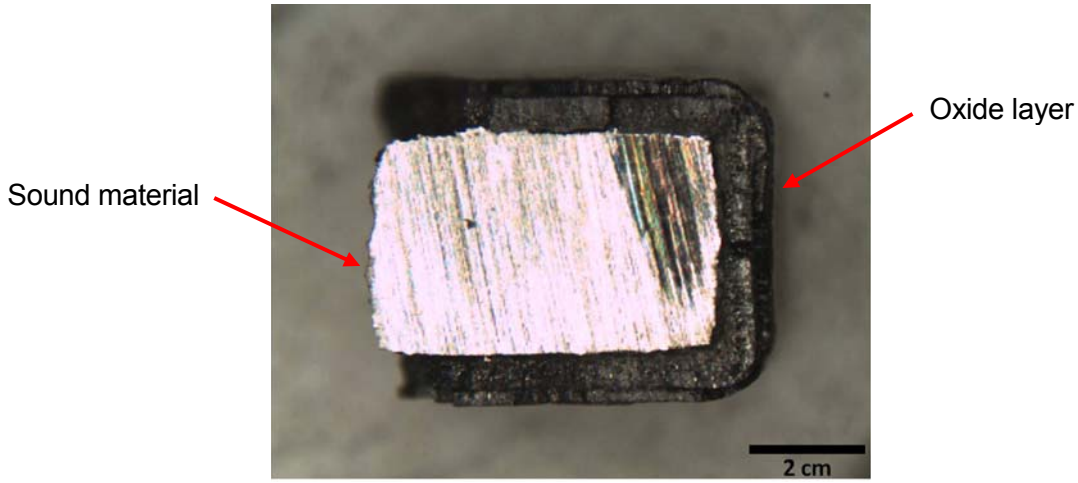

Fig. 4.2. 18%Mn TWIP steel sample heat treated at 1080ºC for 2 hours under controlled atmosphere

TWIP steels were heat treated for one hour at different temperatures as shown in the table D.4.

TWIP steel variety	Treatment duration	Temperatures (°C)
TWIP 18%Mn	1 hour	900, 950, 1000, 1050, 1100
TWIP 20%Mn	1 hour	1100, 1200, 1250
TWIP 25%Mn	1 hour	900, 950, 1000, 1050, 1100

Table D.4. Homogenization heat treatment datas

The homogenization heat treatment was performed following the cycle:

- Rising of the temperature of the furnace up to 1100°C in approximately two hours
- Stabilization of the temperature for a few minutes
- Introduction of the samples for one hour of treatment
- Quenching of the samples in water

This pattern is illustrated in the Fig. 4.3.

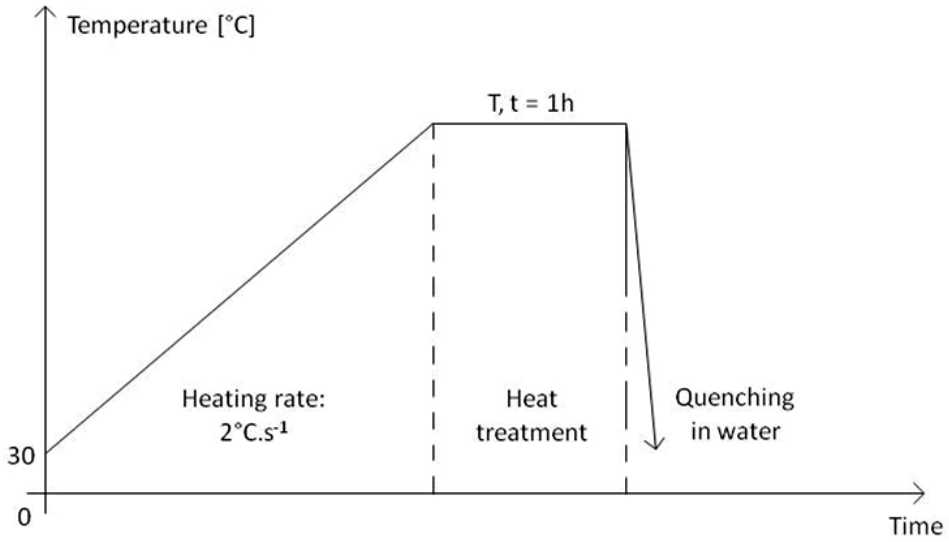

Fig. 4.3. Diagram of the homogenization heat treatment

Another type of homogenization heat treatment was performed for the TWIP steel 18%Mn of two hours long at 1080°C. These specific parameters were submitted by the company doing the heat treatment. One of their clients currently performed such treatments almost every two weeks and it was a save of money to take advantage of it and put our samples at the same time.

4.4. Sample preparation

After heat treatment, the steels were machined into samples to perform hot compression tests, double-hit and stress relaxation tests. Cylindrical samples of 10mm high and a diameter of 5mm were manufactured with the wire electrical discharge machining technique

in the Technological Centre of Manresa (CTM, Manresa, Catalonia, Spain). This machining technique was especially chosen because it doesn't introduce any type of stress

Since stress can cause microstructure transformations or twinning in TWIP steels at the surface, other machining processes could not be used. The initial microstructure before testing should be free of phase transformation or twinning so that mechanical deformation mechanisms could be studied without an initial error.

4.5. High temperature tests

High temperature tests were performed in the Technological Centre of Manresa (CTM, Manresa, Catalonia, Spain) with a *dilatometer 805 Bähr* (Fig. 4.4) which can work at a maximum temperature of 1500°C. To test TWIP steel, alumina (Al_2O_3) punches and pushrods were used and tests were carried out under controlled atmosphere using an inert gas, argon.

Before testing the material, the oxide layer formed during the machining of the samples had to be removed by a soft polishing. The samples are then cleaned in acetone and introduced for a few minutes in an ultrasonic cleaner to remove any dirt such as the oil used to stock them. The oxide layer has to be removed to allow a better adhesion of the thermocouple which measures the temperature of the sample during hot compression testing. It is quite important to pay attention to thermocouple welding because its breakage is one of the most frequent reasons of failure of hot compression tests.

Fig. 4.4. Dilatometer 805 Bähr used for hot compression tests

The thermocouple is spot welded to the sample with a current of 6mA during 3ms. Two plates of molybdenum are also spot welded on the bases of the cylindrical samples to prevent any friction during testing.

When samples were ready, they were carefully placed inside the dilatometer (Fig. 4.5) and centered between the punches. Then the thermocouple was connected to the machine to record the temperature, and the difference in length was set at zero. Before blowing argon, the chamber was emptied up to a vacuum of 5.10^{-4} mbar. Argon is then introduced to have a pressure of 0.2bar in the chamber. Before launching the test, levels of refrigerating water and argon had to be checked.

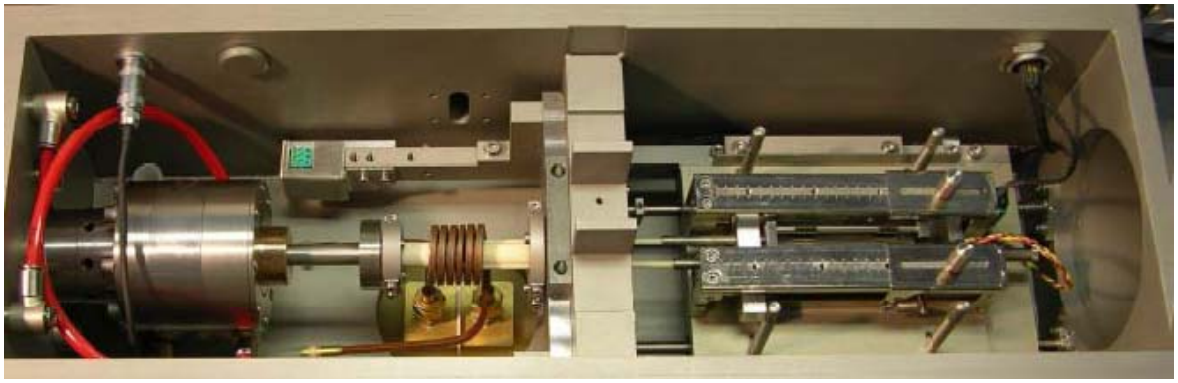

Fig. 4.5. View of the dilatometer's chamber

Then the test cycle was set with the software controlling the dilatometer. Double-hit and relaxation tests last normally half hour.

To characterize static recrystallization in TWIP steels, double-hit and stress relaxation tests were performed in the dilatometer located in Manresa.

4.5.1. Double-hit tests

During double-hit tests, samples were first heat treated at 1100°C for 5 minutes and then the temperature was lowered to the working temperature at a cooling rate of $2°C.s^{-1}$. When the testing temperature was reached, samples were maintained at this temperature for 5 minutes and then the first deformation was applied; the sample was deformed at a constant strain rate of $0.1s^{-1}$ up to a deformation of 0.2. After this deformation stage, the load was released for a time t_i called the interpass time and the working temperature was maintained. This interpass time ranged between 1s and 200s. Finally a second deformation was applied at the same strain rate, $0.1s^{-1}$, up to a deformation of 0.4. After this last deformation, the sample

was quenched by blowing argon. This testing pattern is schematized in the following figure (Fig. 4.6).

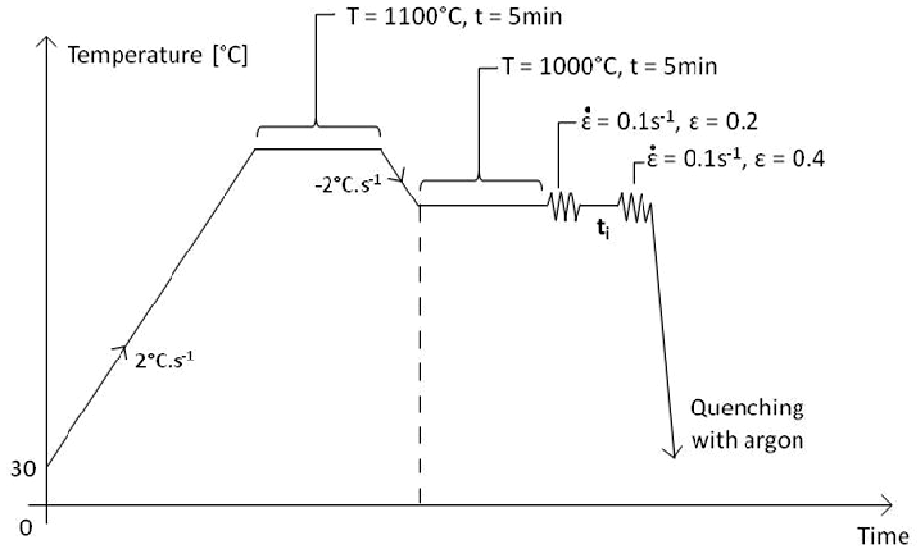

Fig. 4.6. Diagram of a double-hit test thermomechanical schedule for a testing temperature of 1000°C

4.5.2. Relaxation tests

Like in the previous test samples were heat treated before being tested. After 5 minutes at the working temperature, samples were loaded at a certain strain rate up to a chosen deformation. Then, when the deformation was reached, the samples were maintained at this specific value of deformation and the stress relaxation started. Stress vs. time data was recorded for a certain time, which should be long enough to register any strengthening or softening mechanisms which might be taking place inside the material. After relaxation, the samples were quenched by blowing argon in the dilatometer's chamber. The testing schedule is schematized in the following figure (Fig. 4.7).

The relaxation time was set 600s, since this time was sufficient for the steel to be fully relaxed. However, some samples were quenched at intermediate times of 50s, 100s, 200s and 500s, to perform later metallographic characterization and evaluate the progress of recrystallization at each time.

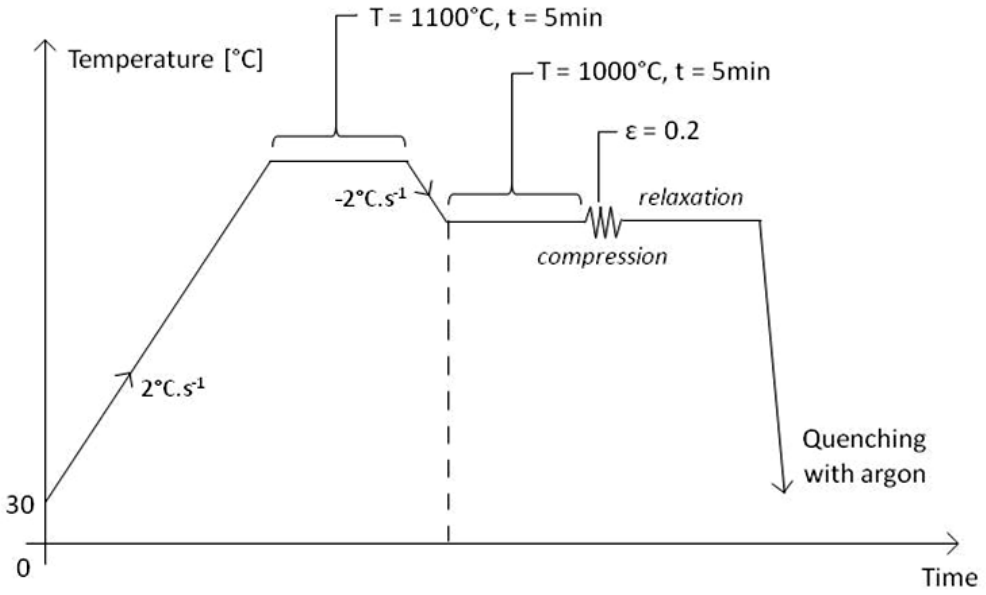

Fig. 4.7. Diagram of a stress relaxation test conducted on a TWIP steel at a temperature of 1000°C after a heat treatment of 5 min at 1100°C

4.6. Metallographic evaluation

Multiple metallographic evaluations were performed for this project. Metallography was used to characterize the state of the material at different stages of the manufacturing of the material or to study the microstructure during and after a mechanical test.

4.6.1. Sample preparation

(i) **As-hot rolled state:** three small pieces of 18%Mn and 25%Mn TWIP steel were cut to characterize the microstructure of the three directions after hot rolling. Direction 11 is the rolling direction. Direction 22 is transverse to the rolling direction and direction 33 is longitudinal to the rolling direction, as shown in the Fig. 4.8.

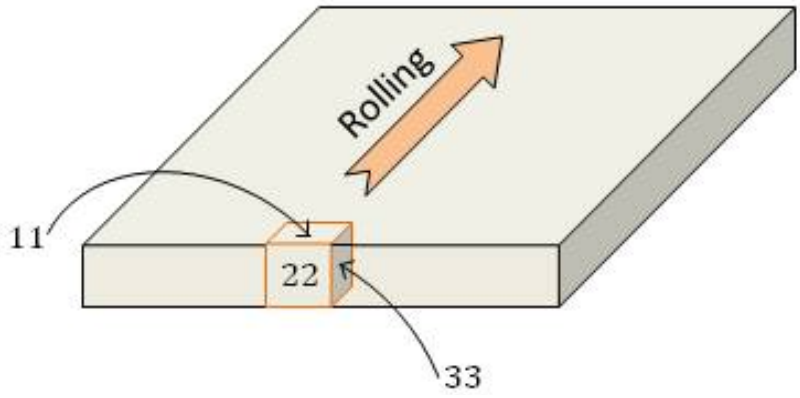

Fig. 4.8. Extraction of the samples in the initial plate

(ii) **After hot compression tests:** Each sample was cut two times to observe the two directions: longitudinal and perpendicular to the compression axis (Fig. 4.9).

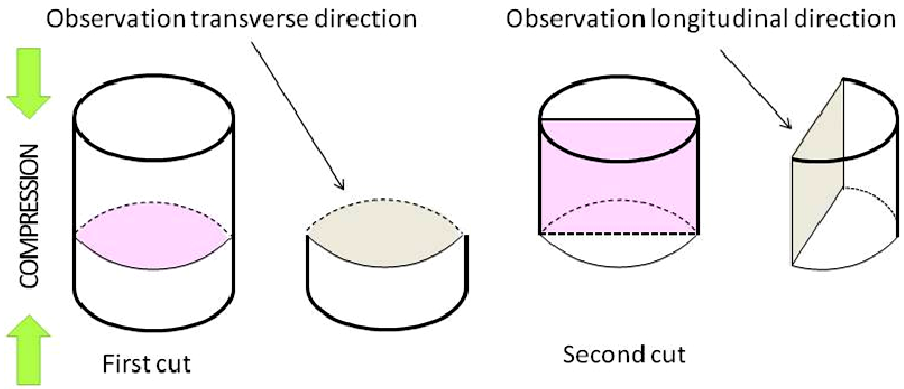

Fig. 4.9. Sample faces observed for microstructure characterization after hot compression testing

4.6.2. Metallographic technology

To prepare the samples for microscopic observation the following stages were realized.

(i) **Cutting:** The compression samples and the initial material were cut with an abrasive cutter Delta ArasiMet, Bruehler with an alumina disc.

(ii) **Coating:** The samples were mounted in black Bakelite with a coating machine Struers, LaboPress-3, with a load of 40N, heated 5 minutes and cooled 3,5 minutes

(iii) **Grinding:** This stage removed the oxide layer formed on the surface of the sample. Silicon carbide abrasive papers of 240, 400, 600, 1200 and 2500 grains were used. It was important to pay attention to the flatness of the surface for further microscopic observation.

(iv) **Polishing:** To obtain a mirror finish, the samples were polished with lubricant and diamond grit in suspension of 9μm, 6μm, 3μm and 1μm. If the samples contained many inclusions, drops of soap could be added. During this stage, the polishing support has to be very clean to prevent any scratch. On the top of it, the sample had to be cleaned very quickly just after polishing otherwise a thin oxide layer was formed on the surface. To clean the sample, it had to be put under running water, sprayed with pure methanol and finally softly wiped with a tissue.

(v) **Etching:** This last stage is necessary to reveal the microstructure. A 2.5% nital solution (2.5% nitric acid and the balance with pure methanol) was heated up to 80°C. Then the sample is also slightly heated before diving it into the etching solution. When the microstructure was revealed, the sample was sprayed with pure methanol to stop the etching and finally dried by blowing hot air.

Etching of the samples could fail easily. The most important parameters were the following:

- Grain size: when the grains were very small, the etchant had to be low concentrated (2.5%); on the contrary if the grains were big, the etchant had to be more concentrated (5%-8%).

- The methanol had to be pure otherwise a thin layer of dirt formed on the surface preventing any microscopic observation.

- Temperature of the etchant and the duration of the attack were also important.

To obtain a satisfactory preparation of the samples, it was often necessary to polish and etch twice. The samples oxidized quite quickly, therefore, microscopic observations had to be done within a few days after preparation. To reduce the oxidation, the samples were placed in desiccators.

4.6.3. Microscopes

4.6.3.1. Optical microscope

To observe the microstructure and take pictures of it, an optical microscope *Buehler Omnimet 5.1* was used. Since some microstructures were better revealed with polarized light, the optical microscope *Reichert MEF-4M* was used to perform these specific pictures.

4.6.3.2. Scanning Electron Microscope

Photos with a high magnification were taken with a *SEM Jeol JSM 6400*. No special preparation had to be done to the samples for the observation with the SEM since TWIP steels are conductive.

4.6.4. Grain size determination

For the 18%Mn and 25%Mn steels, grain size was determined manually by linear intercept method. For each material and temperature more than 250 grains were taken into account to have a representative average.

For the 20%Mn steel, the grain was evaluated thanks to the software *Micron Image Processing*. This image analyzer gave the distribution of the grains diameters so that the equivalent diameter of each sample could be calculated.

This evaluation was very important to determine the effect of the homogenization heat treatment on the microstructure.

4.7. Microhardness test

An *Akashi hardness testing machine* was used to measure the hardness of the steel after it had been heat treated. Vickers indentations were performed to characterize the hardness of each sample on which were realized at least 7 measures with a load of 200mN.

5. Results and discussion

5.1. Mechanical and microstructure characterization at room temperature

5.1.1. As-hot rolled state

In the following table (Table E.1) the rolled state of each steel are presented.

Rolled state, observation in the rolling direction 11, **18%Mn TWIP steel**	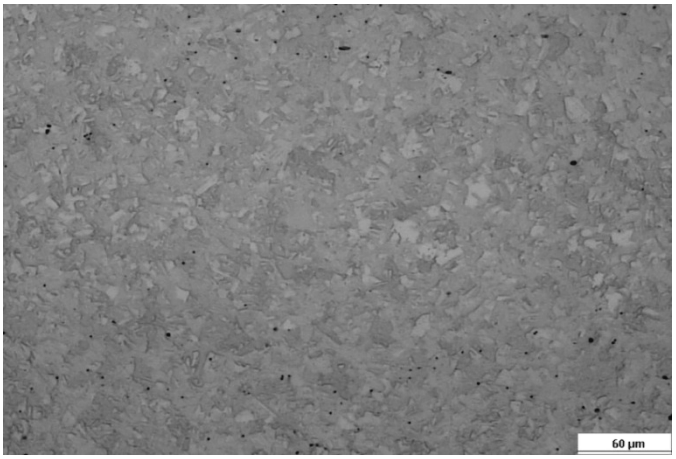 *18%Mn steel observed with optical microscope*
Rolled state, observation in the rolling direction 11, **20%Mn TWIP steel**	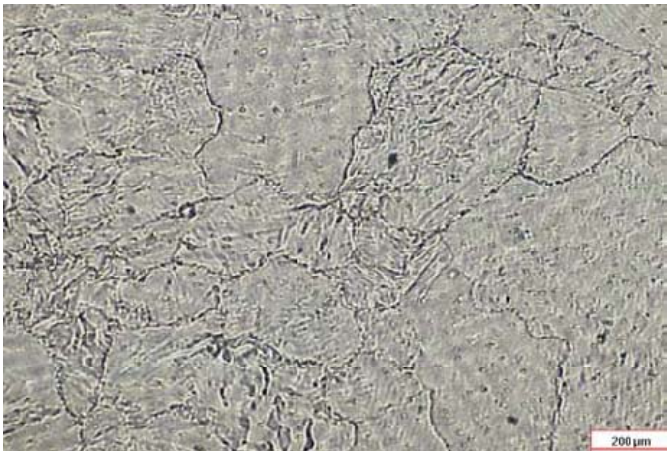 *20%Mn steel observed with optical microscope*

Rolled state, observation in the rolling direction 11, **25%Mn TWIP steel**	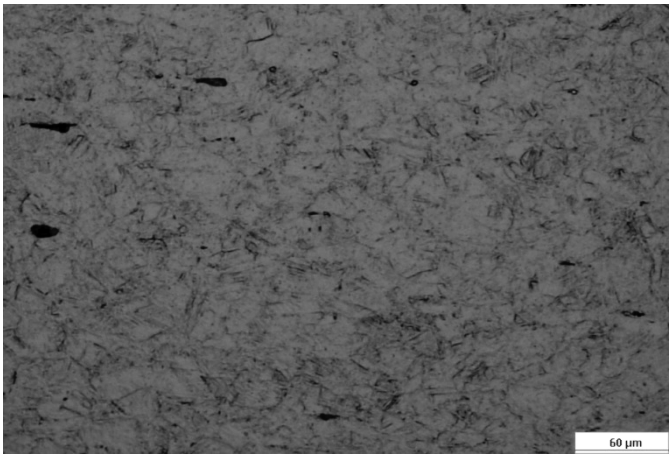 *25%Mn steel observed with optical microscope*

Table E.1. Chemical compositions of the three TWIP steel varieties

Both hot rolled microstructure of 18% and 25%Mn steels present very small grains whereas the 20%Mn steel has a coarser microstructure. This difference comes from the rolling parameters. 18% and 25%Mn steels were hot rolled in LMT-CANMET in Ottawa and 20%Mn steel has been hot rolled in The Metallurgical Research Institute in Mexico.

5.1.2. Tensile tests

Tensile tests were performed on the 20%Mn TWIP steel to have knowledge of its behavior at room temperature while submitted to traction. Samples were deformed at a strain of 3%, 30% and up to final breaking. (see curves Fig. 5.1)

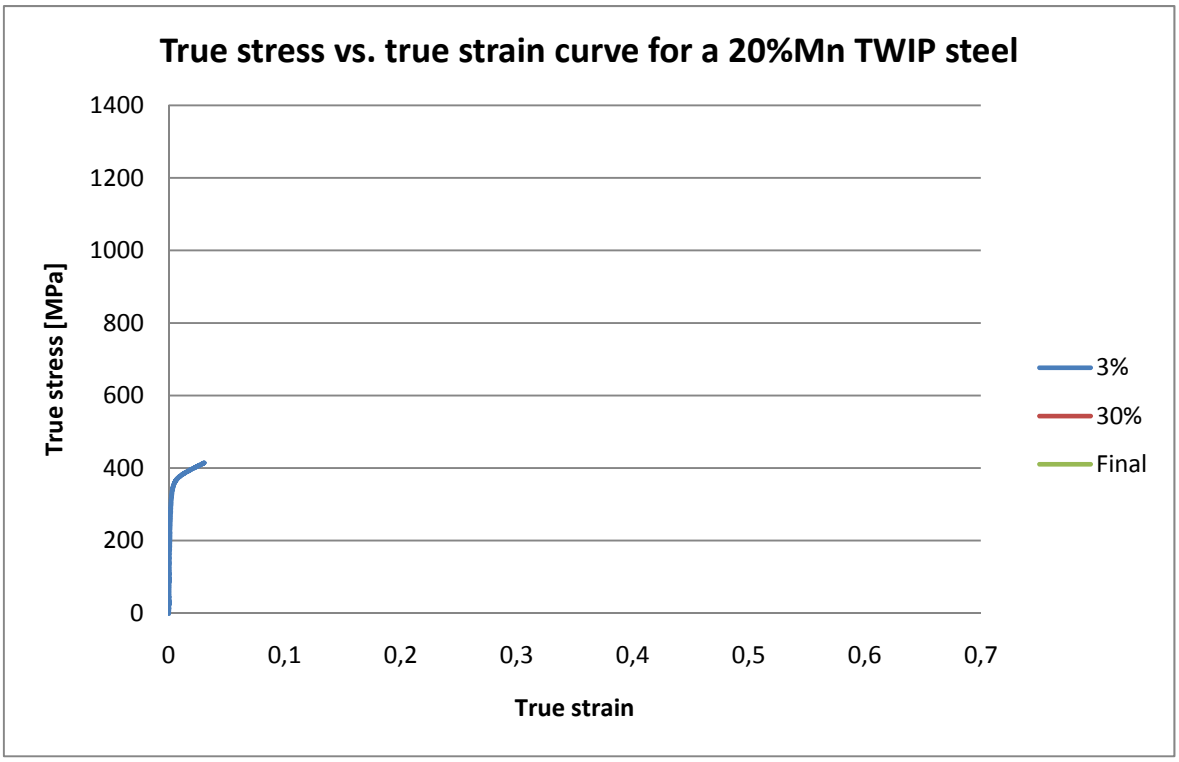

Fig. 5.1. Traction tests performed at room temperature on a 20%Mn TWIP steel, at 3%, 30% and up to breaking

This curve shows that this 20%Mn TWIP steel can be deformed up to a strain of 0.6 and its tensile stress is about 1300MPa. The total elongation is normal for a TWIP steel but the tensile strength is very high in comparison with other TWIP steels reported in the literature.

Metallographic evaluation was performed to see the behavior of the 20%Mn TWIP steel microstructure at different deformation stages at room temperature. Four samples were analyzed at 0%, 3% and 30% deformation and after breaking (Fig. 5.2, 5.3, 5.4 and 5.5):

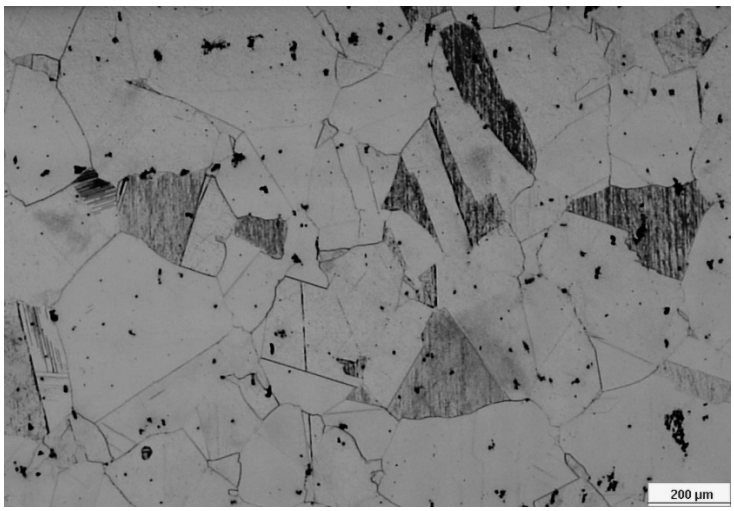

Fig. 5.2. 20%Mn TWIP steel observed with OM at 0% deformation (initial state)

This analysis was performed to study the initial microstructure that was going to be deformed by traction at room temperature. Grains are more or less all the same size and only annealing twins, caused by the heat treatment before manufacturing the samples, are visible.

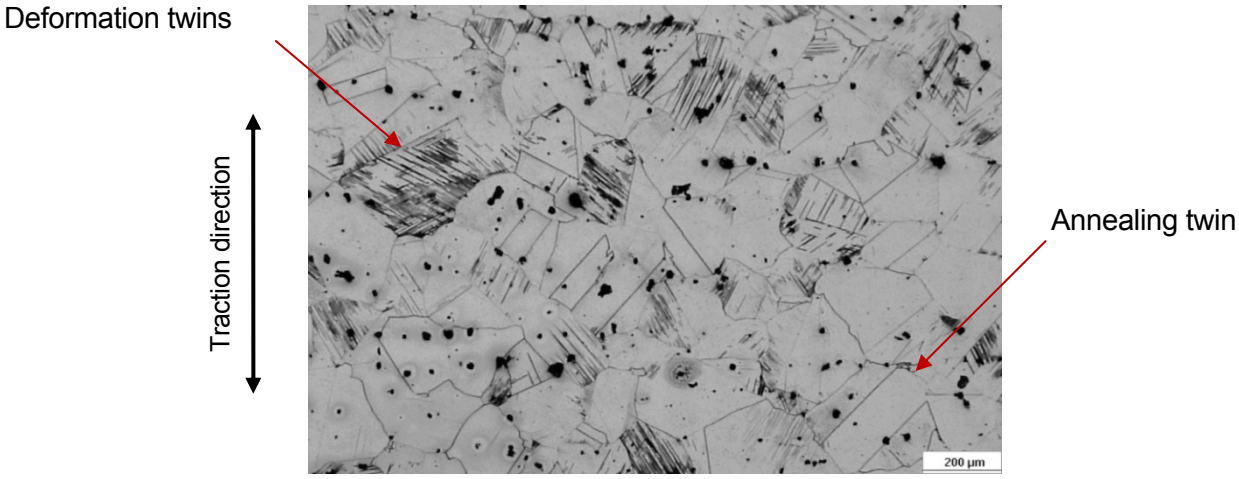

Fig. 5.3. 20%Mn TWIP steel deformed at 3% observed with OM

After 3% deformation, deformation twins can be observed in some grains. The grains are still equiaxed and several annealing twins are visible (Fig. 5.3)

At 30% deformation, the change in microstructure is visible. Grains are stretched in the traction direction and many twins are formed by deformation (Fig. 5.4)

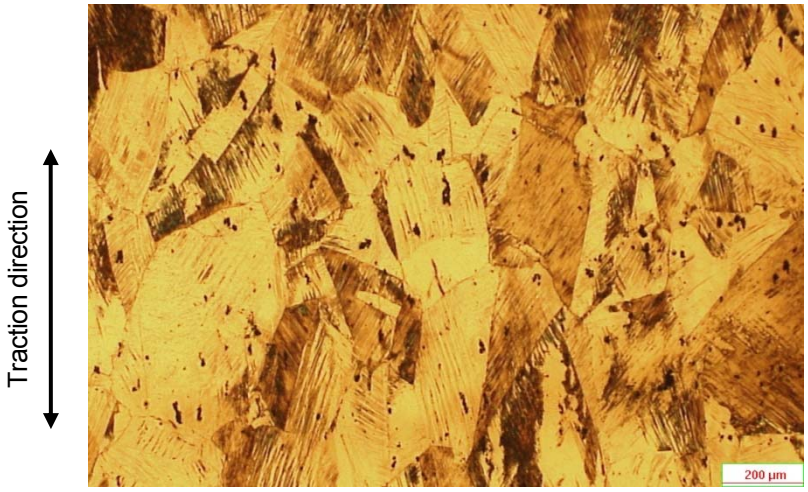

Fig. 5.4. 20%Mn TWIP steel deformed at 30% observed with OM

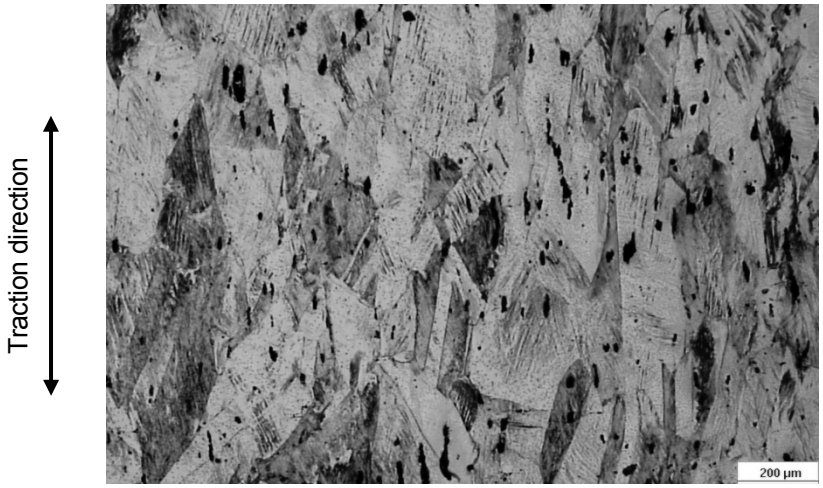

Fig. 5.5. 20%Mn TWIP steel deformed up to breaking observed with OM

In the final state, after breaking of the sample, the microstructure is fully oriented. The traction test produces a texture in the material (Fig. 5.5)

The microstructure analysis of these samples confirms that the principal deformation mode is twinning. Annealing and deformation twins were observed with SEM (Fig. 5.6)

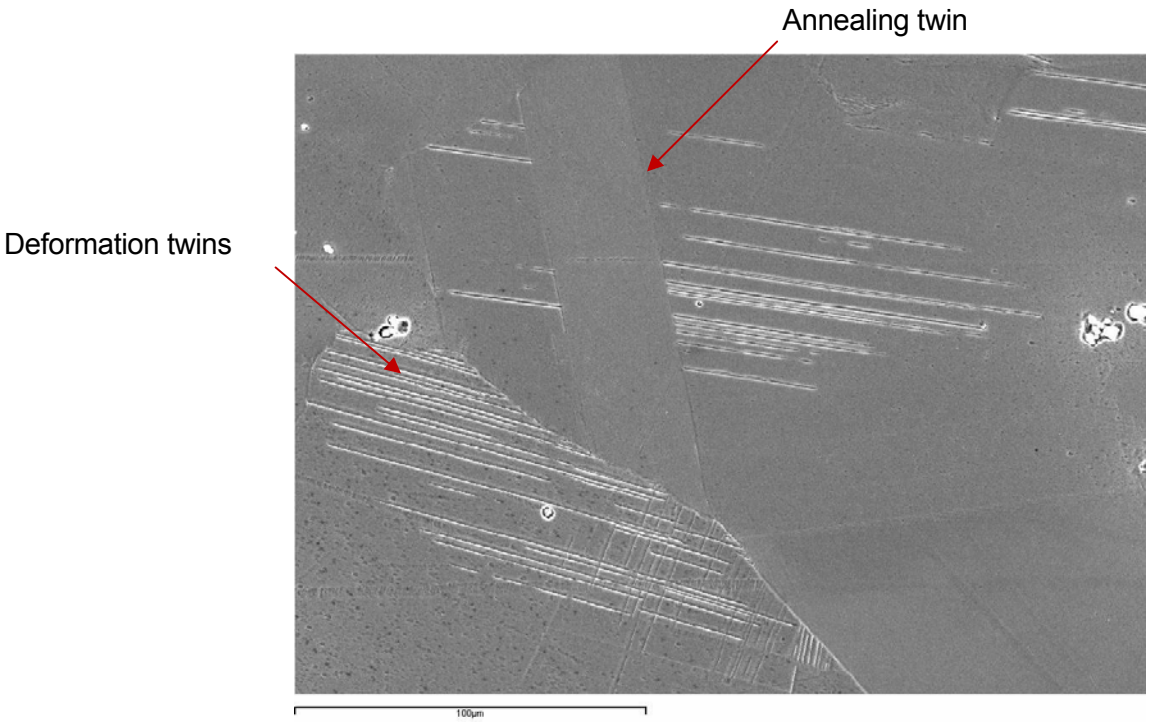

Fig. 5.6. 20%Mn TWIP steel deformed at 3% observed with SEM

5.2. Effect of homogenization heat treatment on microstructure

In the industry, slabs are heat treated before hot rolling to homogenize the microstructure and ease deformation. In this work, homogenization heat treatments will be applied to the samples previous to mechanical testing. Therefore, the first of the work was to determine the effect of heat treatment on the microstructure of TWIP steels by metallographic observation, microhardness measurements and grain size evaluation.

5.2.1. Effect of homogenization heat treatment on microstructure

The TWIP steels were heat treated at different temperatures for an hour (see description in Table D.4). In the following figure, the results are presented for the three steel compositions. (Table E.2, Table E.3 and Table E.4)

5.2.1.1. 18%Mn TWIP steel

Homogenization at 900°C – 1h	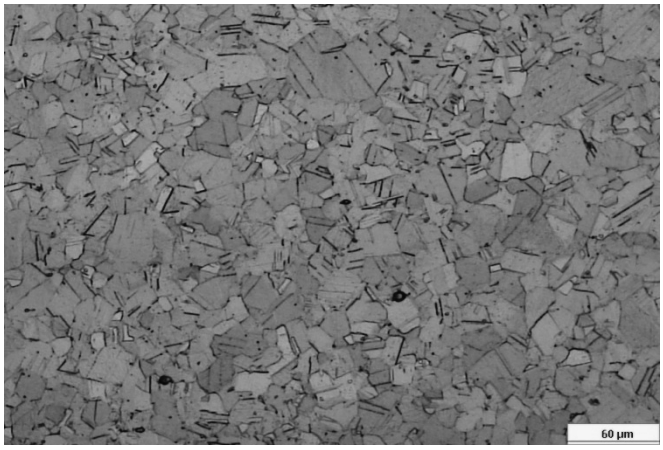 18%Mn TWIP steel microstructure homogenized at 900°C observed with OM

Homogenization at 950°C – 1h	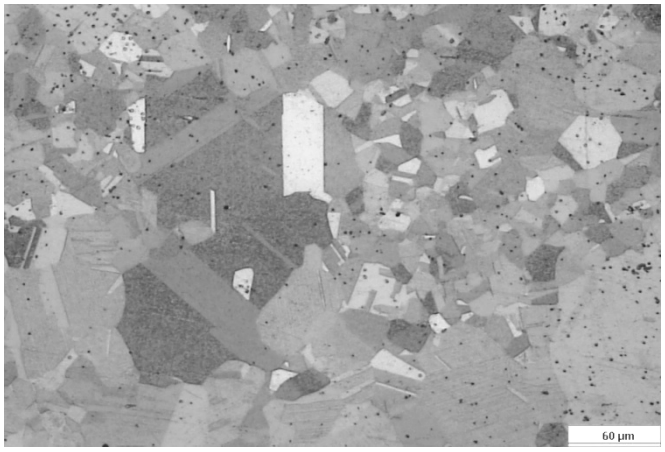 18%Mn TWIP steel microstructure homogenized at 950°C observed with OM
Homogenization at 1000°C – 1h	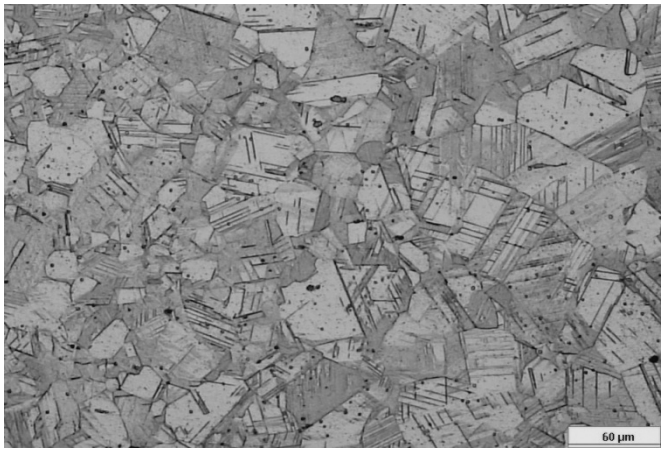 18%Mn TWIP steel microstructure homogenized at 1000°C observed with OM
Homogenization at 1050°C – 1h	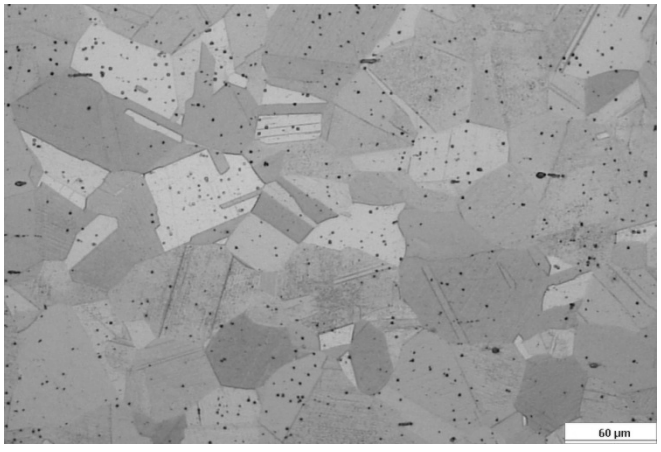 18%Mn TWIP steel microstructure homogenized at 1050°C observed with OM

Homogenization at 1100°C – 1h	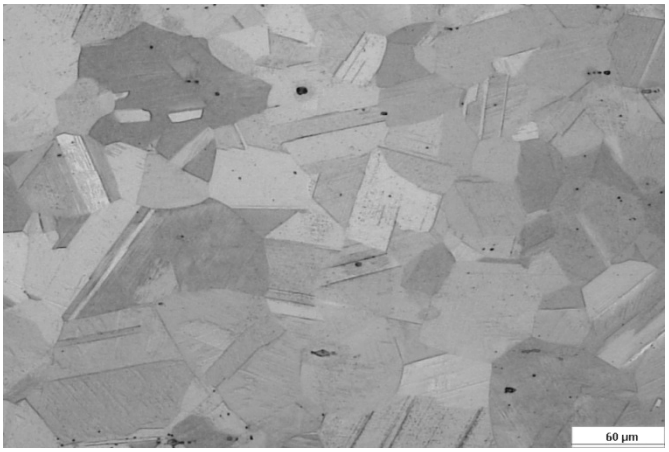 18%Mn TWIP steel microstructure homogenized at 1100°C observed with OM

Table E.2. Microstructure evaluation of the 18%Mn TWIP steel after homogenization

It seems that up up to 1000°C, the steel was not fully homogenized. Some deformation twins due to hot rolling are still visible. 1050°C and 1100°C heat treatment caused grain growth and the formation of annealing twins.

5.2.1.2. 20%Mn TWIP steel

Homogenization at 1100°C – 1h	 20%Mn TWIP steel microstructure homogenized at 1100°C observed with OM

Homogenization at 1200°C – 1h	 20%Mn TWIP steel microstructure homogenized at 1200°C observed with OM
Homogenization at 1250°C – 1h	 20%Mn TWIP steel microstructure homogenized at 1250°C observed with OM

Table E.3. Microstructure evaluation of the 20%Mn TWIP steel after homogenization

At 1250°C, the heat treatment has caused a too important grain growth so this temperature is too high. It seems that the adequate temperature for heat treating the 20%Mn TWIP steel is 1200°C, since this heat treatment generates a homogeneous grains size, only a few annealing twins are evident, and there is no excessive grain growth.

5.2.1.3. 25%Mn TWIP steel

Homogenization at 900°C – 1h	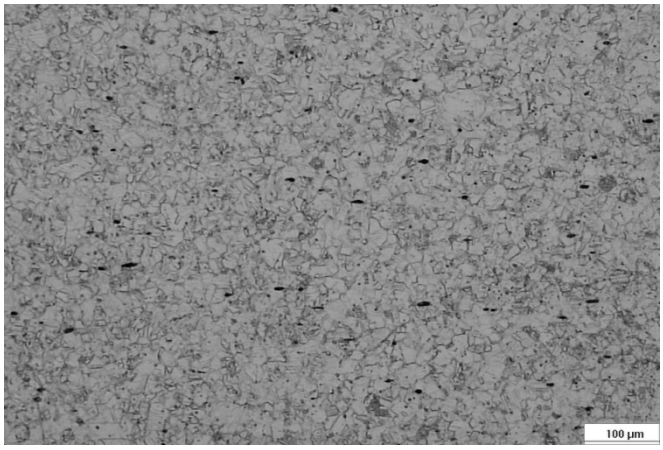 25%Mn TWIP steel microstructure homogenized at 900°C observed with OM
Homogenization at 950°C – 1h	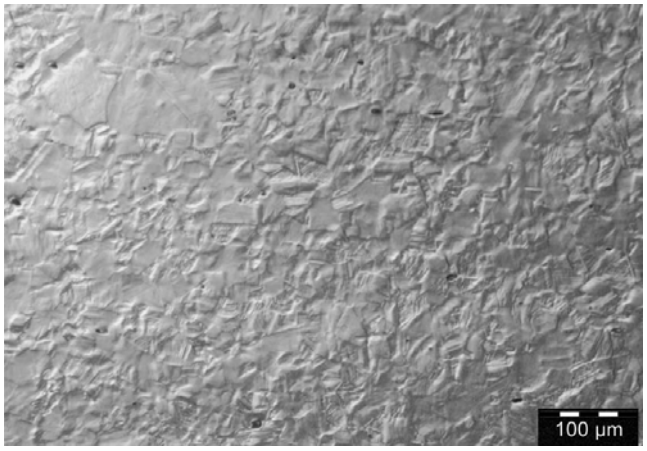 25%Mn TWIP steel microstructure homogenized at 950°C observed with OM (polarized light)
Homogenization at 1000°C – 1h	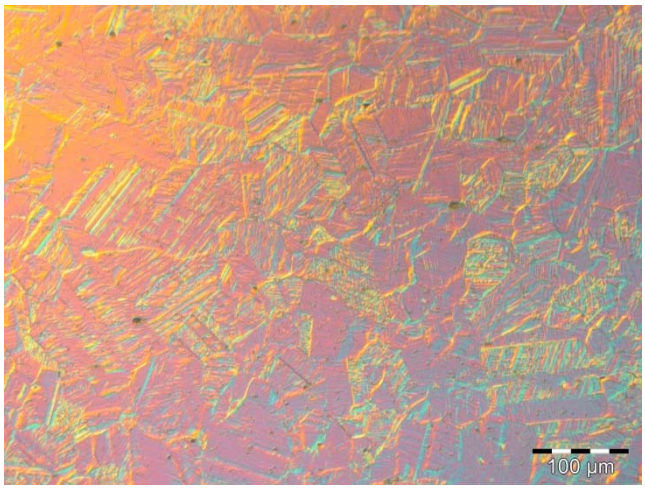 25%Mn TWIP steel microstructure homogenized at 1000°C observed with OM (polarized light)

Homogenization at 1050°C – 1h	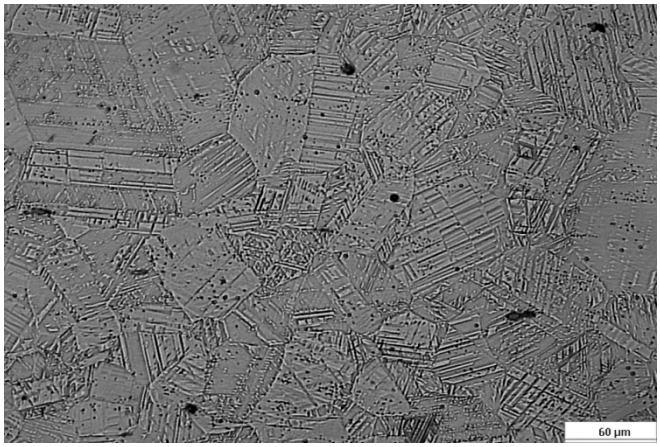 25%Mn TWIP steel microstructure homogenized at 1050°C observed with OM
Homogenization at 1100°C – 1h	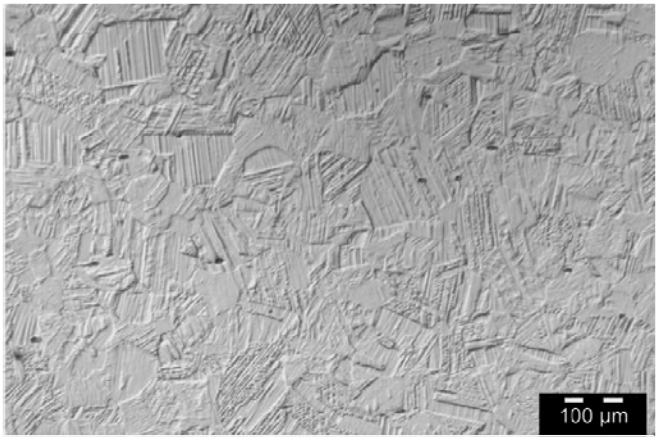 25%Mn TWIP steel microstructure homogenized at 1100°C observed with OM (polarized light)

Table E.4. Microstructure evaluation of the 25%Mn TWIP steel after homogenization

For the 25%Mn TWIP steel, it seems that a heat treatment at 1100°C is not sufficient to remove deformation twins and homogenize the microstructure. This observation can be disturbed by the quality of the metallographic preparation: this grade of TWIP steel was hard to prepare, probably due to the low carbon content and the high manganese content. The best microstructures for this steel were revealed with polarized light.

5.2.2. Grain size evaluation and hardness tests

To complete information obtained with micrographs, microhardness tests and grain size measurements were performed. (Fig. 5.7 to 5.11)

5.2.2.1. 18%Mn TWIP steel

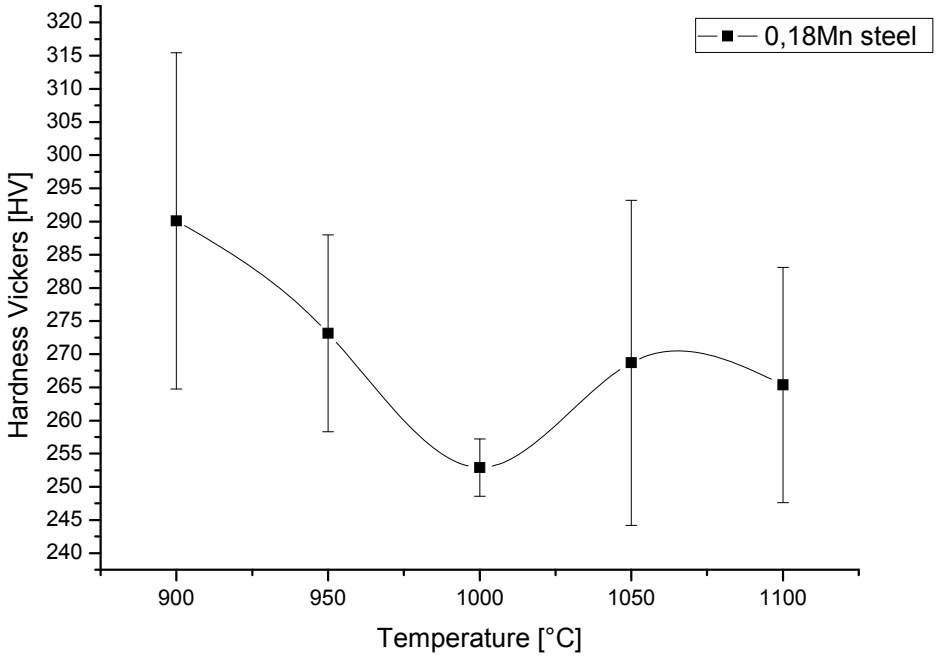

Fig. 5.7. Microhardness evolution with homogenization heat treatment temperature for the 18%Mn TWIP steel

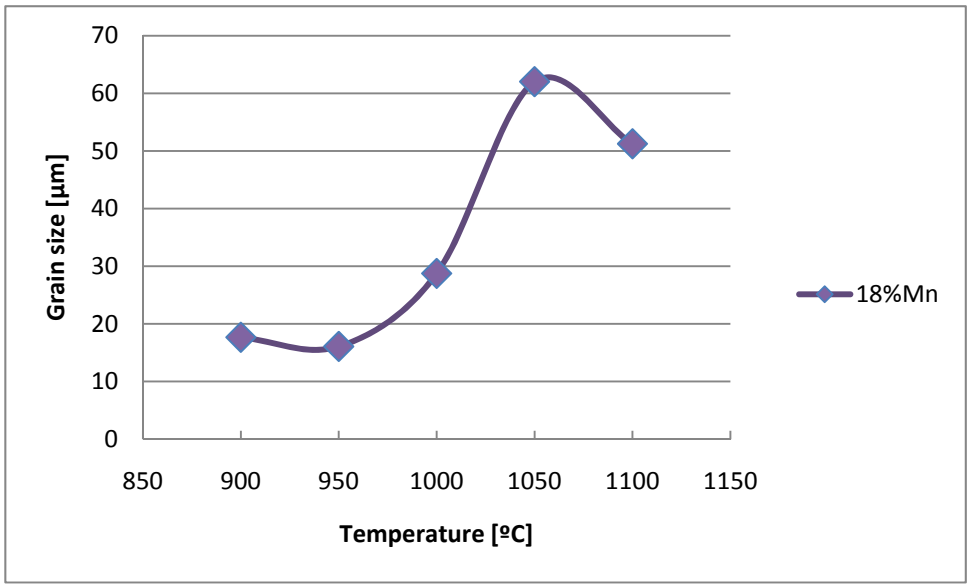

Fig. 5.8. Grain size evaluation on the 18%Mn TWIP steel after homogenization heat treatment at different temperatures

5.2.2.2. 20%Mn TWIP steel

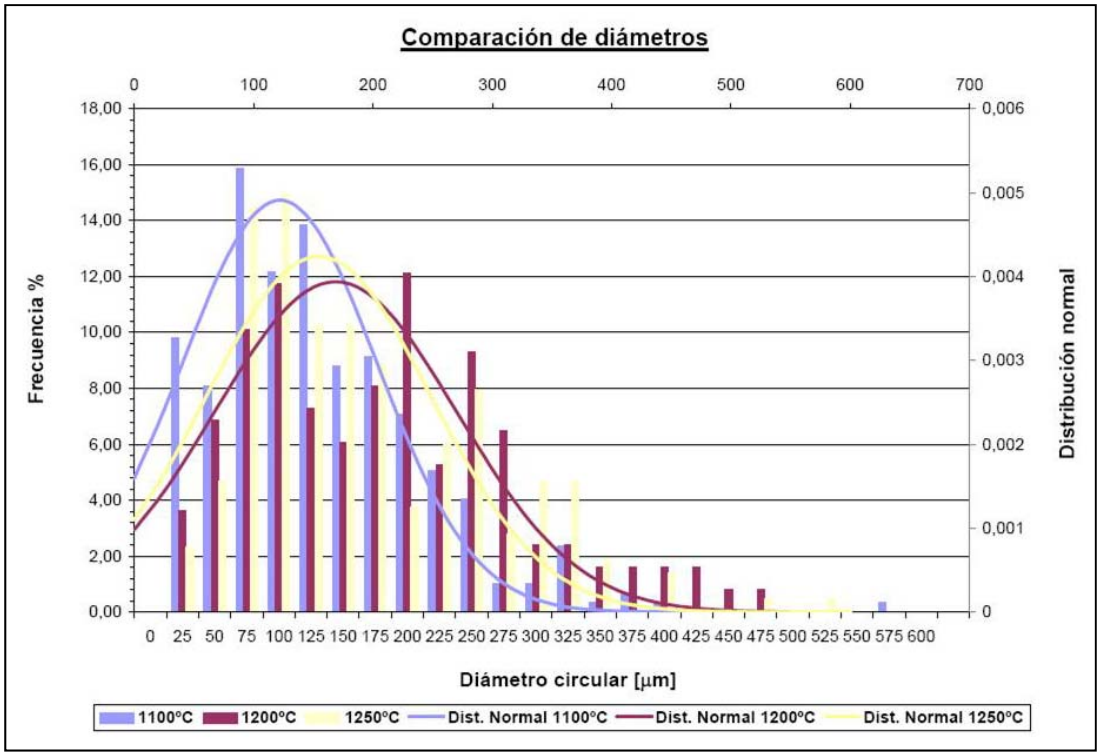

Fig. 5.9. Grain size evolution with homogenization heat treatment temperature for the 20%Mn TWIP steel

5.2.2.3. 25%Mn TWIP steel

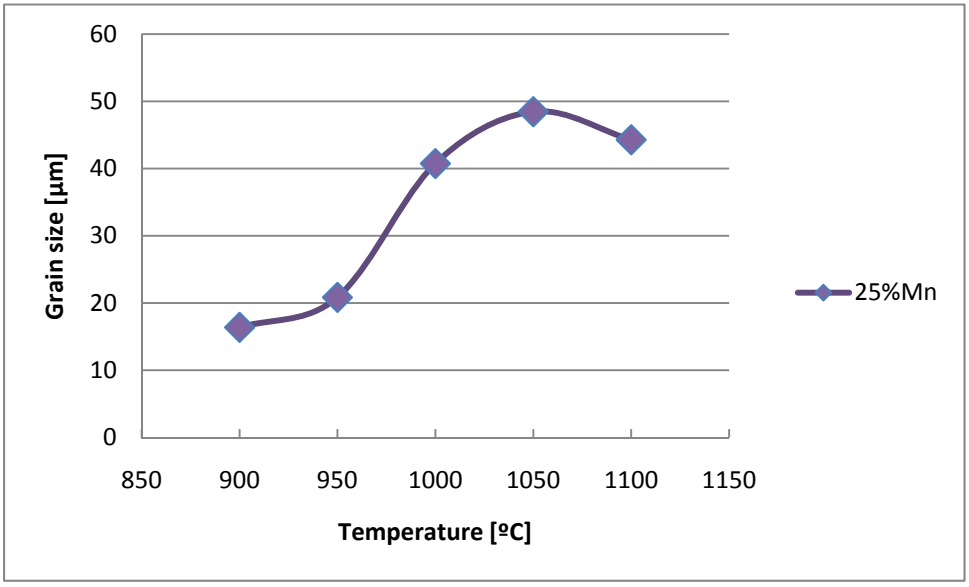

Fig. 5.10. Grain size distribution on the 25%Mn TWIP steel after homogenization heat treatment at different temperatures

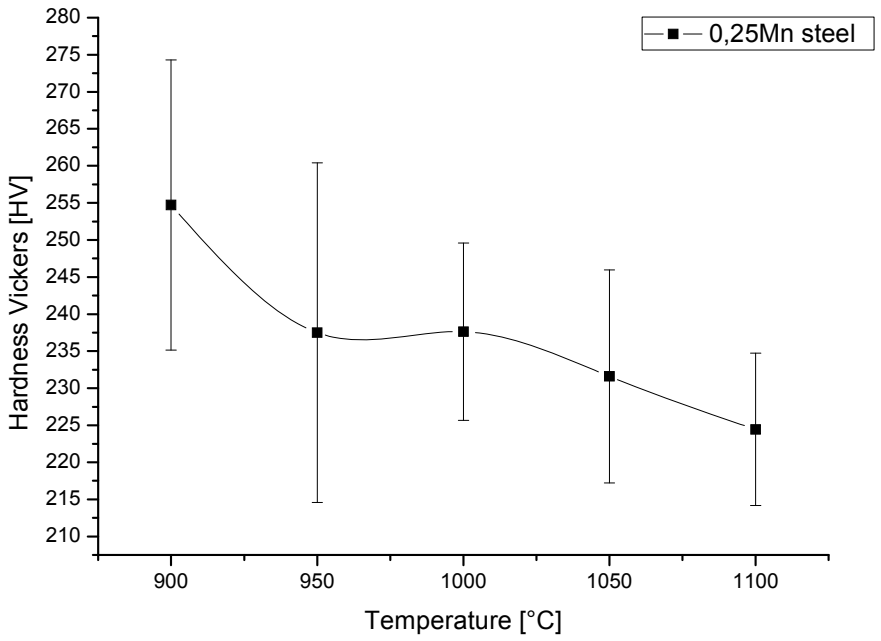

Fig. 5.11. Microhardness tests on the 25%Mn TWIP steel after homogenization heat treatment at different temperatures

The analyses of micrographs and grain size evaluation agree to point out that grain size increase with heat treatment temperature. It can also be noticed that hardness decrease with the same temperature. For the 18%Mn TWIP steel and the 25%Mn TWIP steel it was considered that the optimal temperature for heat treatment is 1100°C, according to these results. For the 20%Mn TWIP steel, 1200°C has been chosen as the optimal temperature. These temperatures are sufficient to generate a new homogenous microstructure free of stresses and at the same time they limit an excessive grain growth.

5.2.3. Comparison

The 20%Mn TWIP steel can't be compared to the 18%Mn and 25%Mn steels since its processing route and microstructure is very different. The 20%Mn steel grains are bigger which is probably due to the cooling stage of the manufacturing process (200μm for the 20%Mn steel and around 50μm for the 18%Mn and 25%Mn steels).

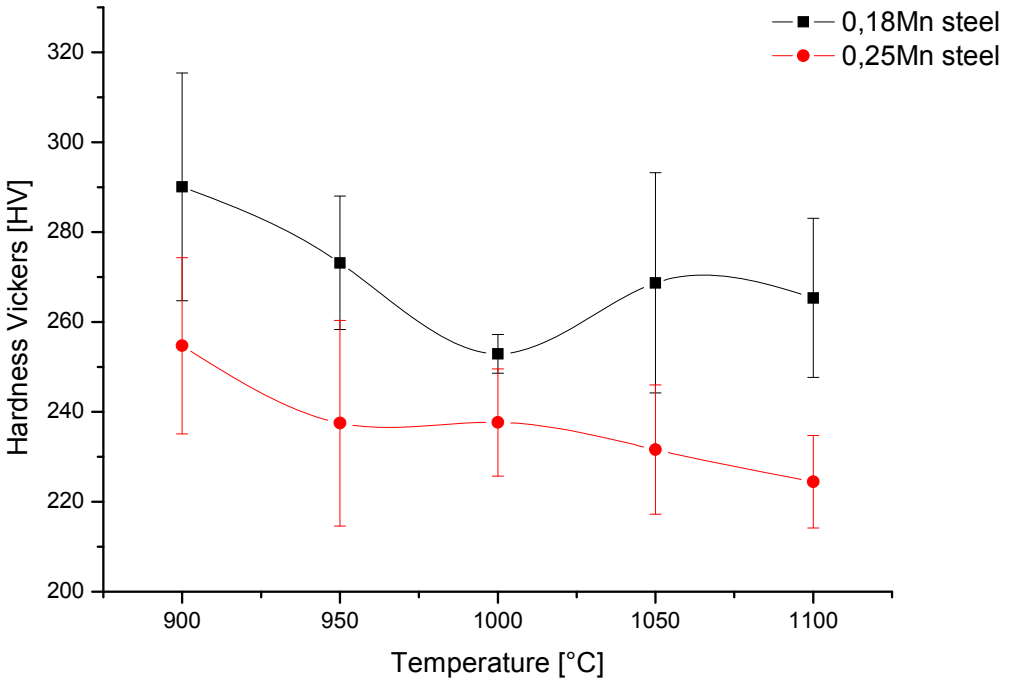

Fig. 5.12. Comparison of Vickers hardnesses in 18%Mn and 25%Mn steels after homogenization heat treatment

This hardness evaluation (Fig. 5.12) reveals that the 18%Mn TWIP steels is harder than the 25%Mn steel after heat treatment. In theory, Mn should be strengthening the material by solid solution. T. Bajor reported about Mn that “Its presence in the alloy in the large quantity increases hardness of the steel and prevents oxides from formation, that means it deoxidises steel in the heat treatment process.” [T. BAJOR, et al., 2007]. Therefore the difference between 18%Mn and 25%Mn cannot be explained in terms of Mn contents.

In fact the higher hardness of the 18%Mn TWIP steel is due to the carbon content which is higher than for the 25%Mn TWIP steel.

Grain size evolution can also be compared between 18%Mn and 25%Mn steel. Their initial grain size was almost the same, around 20µm (Fig. 5.13).

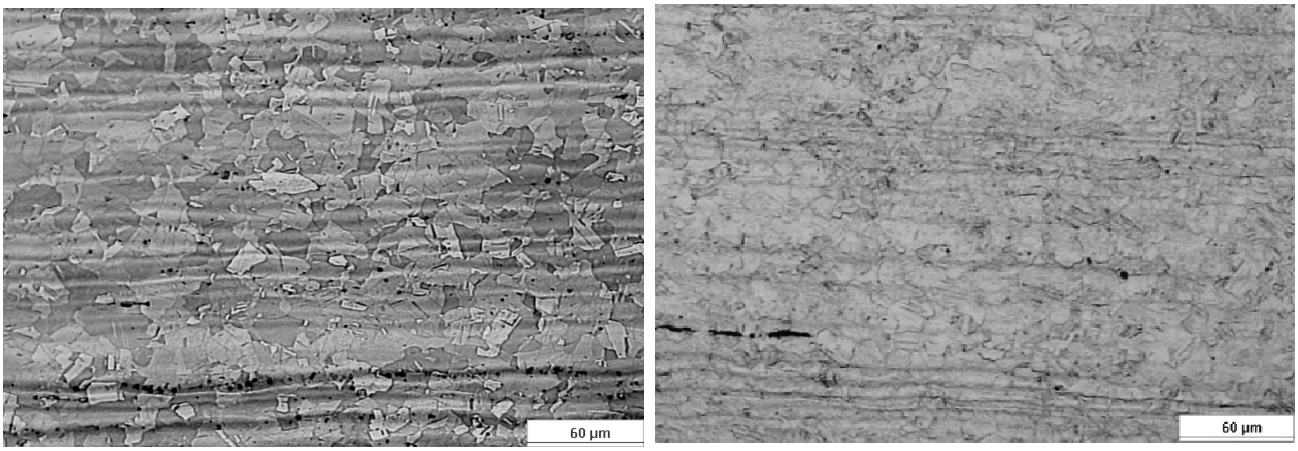

(a) (b)

Fig. 5.14. Rolled state of 18%Mn (a) and 25%Mn (b) TWIP steels observed with OM in the direction 33

It can be considered that the initial microstructure before homogenization heat treatment is a constant parameter for the two studied steels. Moreover, the two steels were homogenized for the same time in the furnace and quenched in water following the same procedure. Therefore, it can be considered that the only parameter that changes is the chemical composition and more precisely the amount of manganese. According to Fig. 5.14, grain size coarsening during homogenization treatment is lower for the 25%Mn. This could be indicating an effect of Mn on retarding the grain growth.

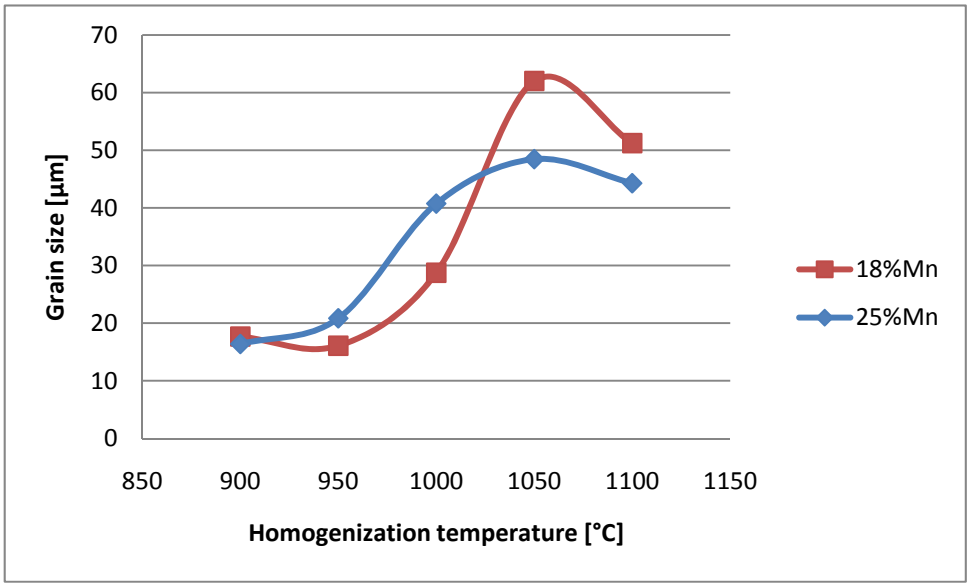

Fig. 5.13. Comparison of change in grain size with homogenizing temperature

5.3. Behavior of a 20%Mn TWIP steel at high temperature

The characterization of the behavior of 20%Mn TWIP steel at high temperatures has been carried out in different stages and this work is the continuation of the experimentation carried out previously by other students. The first part included the characterization of the dynamic restoration processes through the flow curves at different temperatures and strain rates. The results were reported in the work by Rosa Pineda [R. M. PINEDA HUITRÓN, 2009]. Later on, double-hit compression tests were performed by Amandine Delon [A. DELON, 2010] to characterize the static recrystallization of the same alloy. In this work, the previous results have been completed and stress relaxation tests were performed. The differences and ameliorations will be discussed at the end of this section.

5.3.1. Hot flow tests

Hot flow curves were obtained with compression tests at high temperature realized in a dilatometer. Tests were performed at a strain rate of $0.1s^{-1}$ and at the following temperatures: 900ºC, 950ºC, 1000ºC and 1050ºC. (See Fig. 5.15)

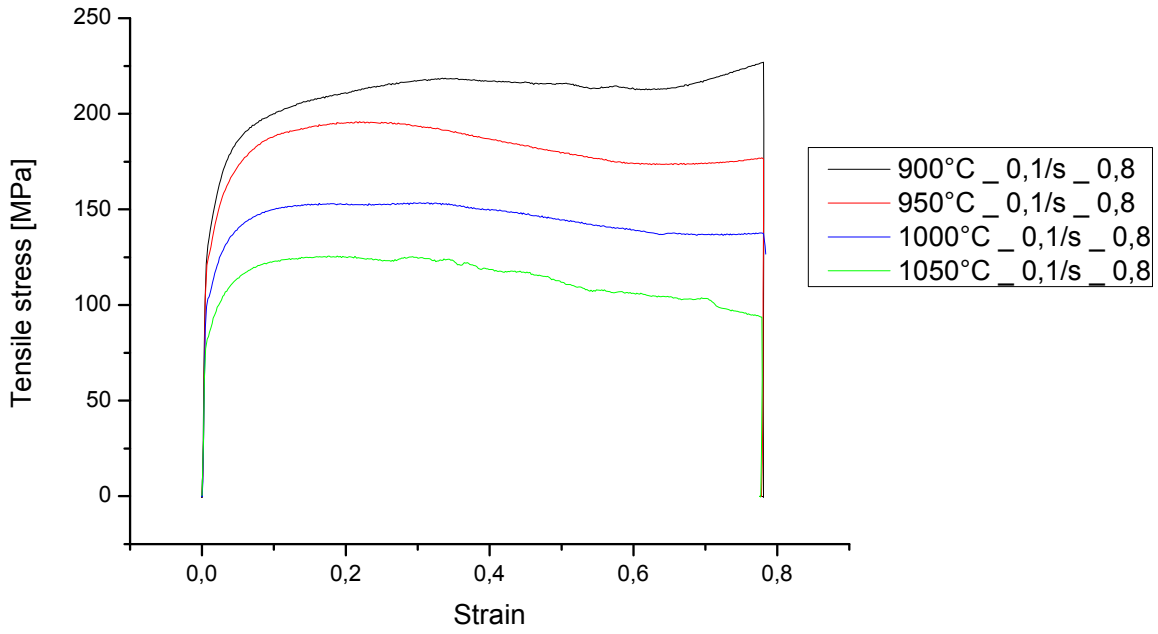

Fig. 5.15. Hot flow curves of a 20%Mn TWIP steel obtained with a dilatometer at a strain rate of $0.1s^{-1}$ and temperatures of 900°C to 1050°C

The quantity of energy brought to the material increases as the temperature increases, therefore less stress is necessary to deform the material, so the curve corresponding to a higher temperature is below a curve that represents a lower temperature. Curves obtained at 950°C, 1000°C and 1050°C present a softening due to dynamic recrystallization, whereas at 900°C it seems that the softening is only due to dynamic recovery. The hot flow curve obtained at 950ºC is typical of a single peak dynamic recrystallization phenomenon.

The flow curves in Fig. 5.19 were specifically obtained for this project, to determine the parameters for double-hit and stress relaxation tests. In particular, when static recrystallization is to be characterized, these curves indicate the conditions of temperature and strain for which assure that no dynamic recrystallization has taken place. However, hot flow curves at temperatures ranging between 800ºC and 900ºC and strain rates from $10^{-1}s^{-1}$ to $10^{-3}s^{-1}$ were previously reported [R. M. PINEDA HUITRÓN, 2009].

5.3.2. Double hit compression tests

The first set of double-hit tests was performed at 900°C, at a strain rate of $0.01s^{-1}$. The first deformation was 0.2 and the second 0.4. Between these two deformations, an interpass time $\mathbf{t_i}$ was modulated between 0.5s and 500s. All the double-hit results under these conditions can be found in Amandine's final project. The double-hit test with an interpass time of 20s is presented on the following figure (Fig. 5.16) as an example.

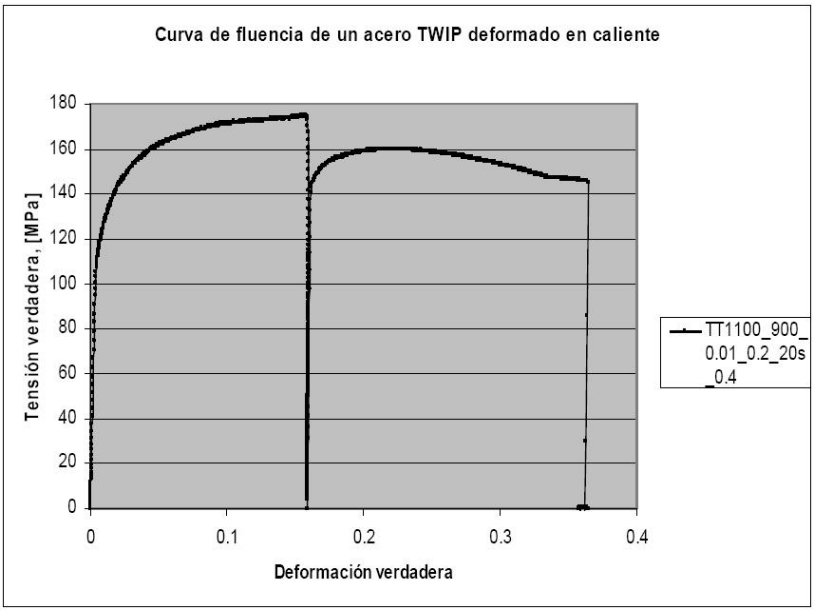

Fig. 5.16. Double hit test performed at 900°C after 5 minutes annealing at 1100°C, with a strain rate of 0.01s-1, a first deformation of 0.2 and a second deformation of 0.4, and an interpass time of 20s.

The recrystallized fraction vs interpass time curve, which represents the static recrystallization kinetics at 900ºC and 0.01s^{-1} were derived from double-hit tests using two different methods, and the results are shown in Fig. 5.17.

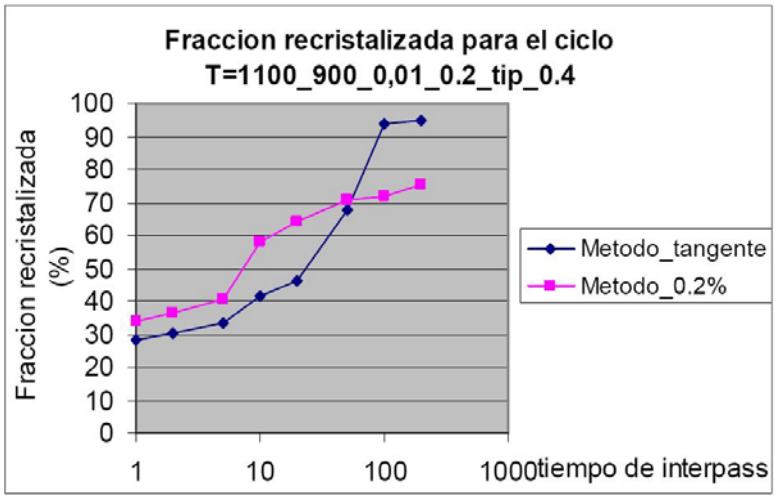

Fig. 5.17. Diagram of recrystallized fraction vs. interpass time. Recrystallized fraction was obtained with double-hit tests

This analytic evaluation gave a recrystallized fraction higher than the fraction obtained by metallography. Nevertheless, this method gives the results expected but requires a lot of tests which means a lot of time, material and consequently money. To overcome these drawbacks and save money, another method has been tried, i.e. using stress relaxation tests to characterize static recrystallization.

5.3.3. Stress relaxation tests

Stress relaxation tests were performed to evaluate if the recrystallized fraction could be estimated from this technique. Once the technique was calibrated, it was used to study the influence of the experimental parameters on recrystallization kinetics. For the calibration, a series of relaxation tests were stopped at different relaxation times and the samples were quenched for metallographic evaluation. The evolution of static recrystallization was determined by optical microscopy means and the results were related to the stress relaxation curve.

5.3.3.1. Calibration technique

This first part aim at estimating the recrystallized fraction which is derived from stress relaxation tests and then compare it with metallographic evaluations. To do so, the stress

relaxation test of reference was performed at 950°C, at a strain rate of $0.1s^{-1}$ and a strain of 0.2 (Fig. 5.18). And then, to see the evolution of the microstructure during the stress relaxation, some samples were quenched before the end of the relaxation.

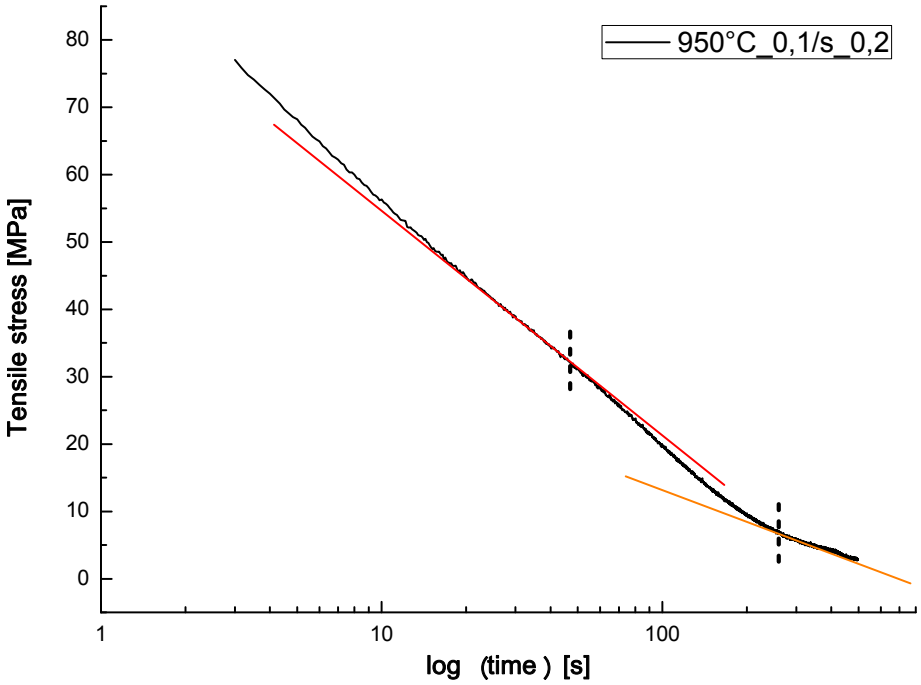

Fig. 5.18. Stress relaxation curve at 950°C, strain rate of $0.1s^{-1}$ and 0.2 strain.

The material seems to relax very little. But it seemed likely to consider that softening was occurring between 48s and 260s. To make sure that a full recrystallization is obtained after 500s relaxation, metallographic evaluations were performed on samples quenched after 50s, 100s, 200s, and 500s of relaxation (Fig. 5.19 to 5.26).

50s of relaxation

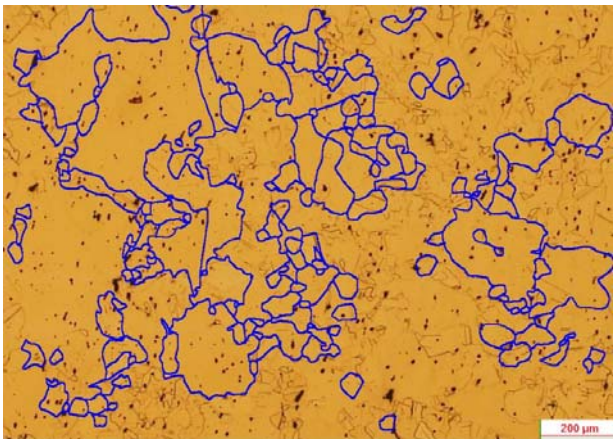

Fig. 5.19. Optical analysis for grain size determination (OM, 05), 950°C, $0.1s^{-1}$, 0.2, 50s relaxation

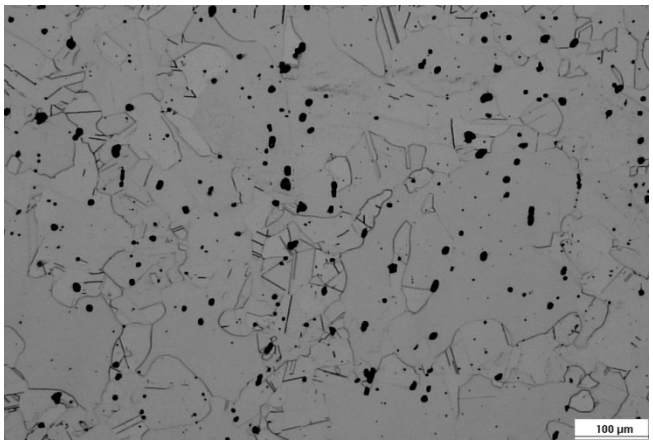

Fig. 5.20. Stress relaxation sample: 950°C, $0.1s^{-1}$, 0.2, 50s relaxation (OM, 10)

After 50s of stress relaxation, it can be observed that recrystallization has already started.

100s of relaxation

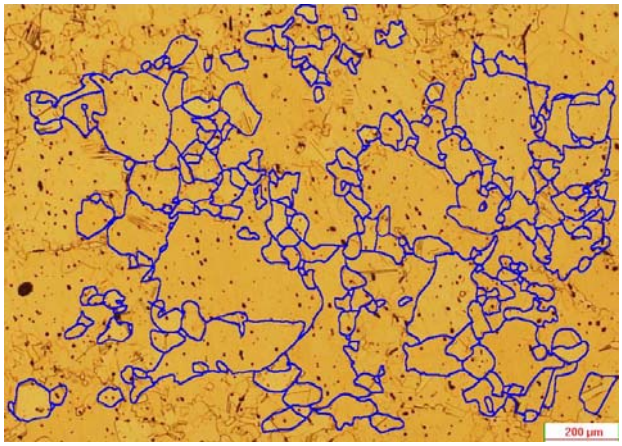

Fig. 5.21. Optical analysis for grain size determination (OM, 05), 950°C, $0.1s^{-1}$, 0.2, 100s relaxation

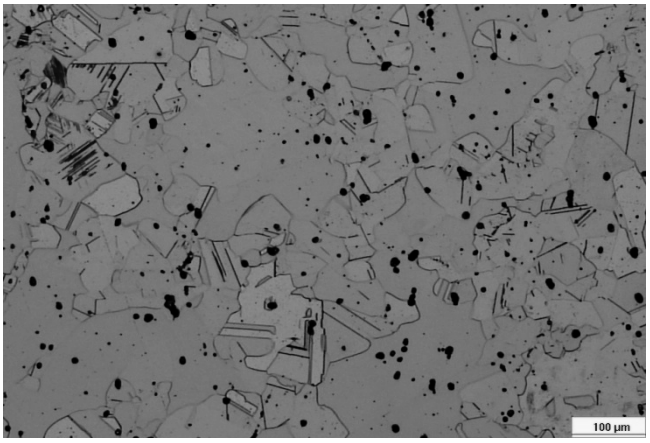

Fig. 5.22. Stress relaxation sample: 950°C, $0.1s^{-1}$, 0.2, 100s relaxation (OM, 10)

The grain size evaluation shows more recrystallized grains after 100s relaxation. There are still big grains which boundaries are preferential locations for recrystallization.

200s of relaxation

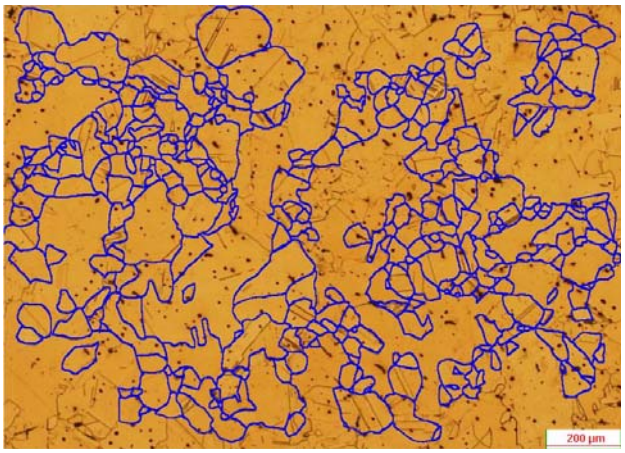

Fig. 5.24. Optical analysis for grain size determination (OM, 05), 950°C, $0.1s^{-1}$, 0.2, 200s relaxation

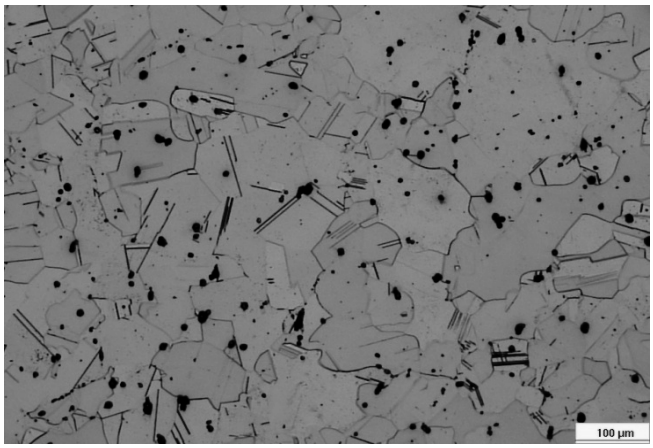

Fig. 5.23. Stress relaxation sample: 950°C, $0.1s^{-1}$, 0.2, 200s relaxation (OM, 10)

The microstructure is almost fully recrystallized after 200s relaxation, and the recrystallized grains are quite small. In the Fig. 5.24, many twins can be observed in some coarse grains, which means that the recrystallization has not finished yet.

500s of relaxation

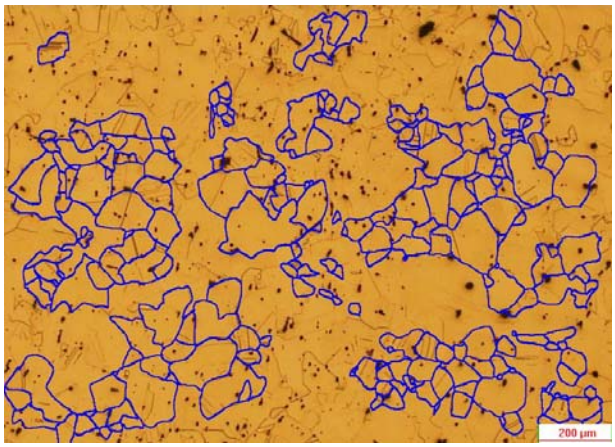

Fig. 5.25. Optical analysis for grain size determination (OM, 05), 950°C, $0.1s^{-1}$, 0.2, 500s relaxation

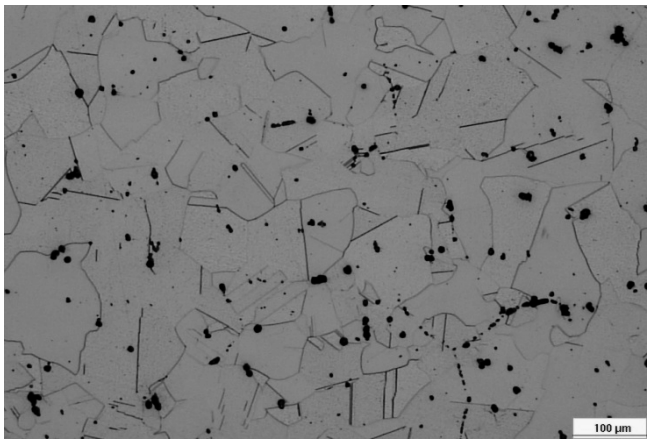

Fig. 5.26. Stress relaxation sample: 950°C, $0.1s^{-1}$, 0.2, 500s relaxation (OM, 10)

After 500s relaxation, the microstructure is almost homogenized. Grains are a little bit bigger than after 200s relaxation, which is due to grain growth. On the picture taken at higher

magnification (Fig. 5.26) the microstructure seems to be fully recrystallized. A few annealing twins can be observed inside the grains.

Longitudinal cuts were also performed and metallographic evaluations realized, for the samples quenched after 50s, 100s, 200s and 500s. All the pictures are shown in appendices for a matter of size of the pictures. The pictures are in big dimensions to be able to observe the gradient in the microstructure between the outside of the sample and the middle where the transverse cut had been realized.

It can be considered that after 500s relaxation at 950°C, the microstructure has fully recrystallized. Therefore, the changes is the slope of relaxation curve can be related to the beginning and the end of recrystallization and the corresponding stresses can be used in the equation 3.6 to determine the recrystallized fraction (Fig. 5.27).

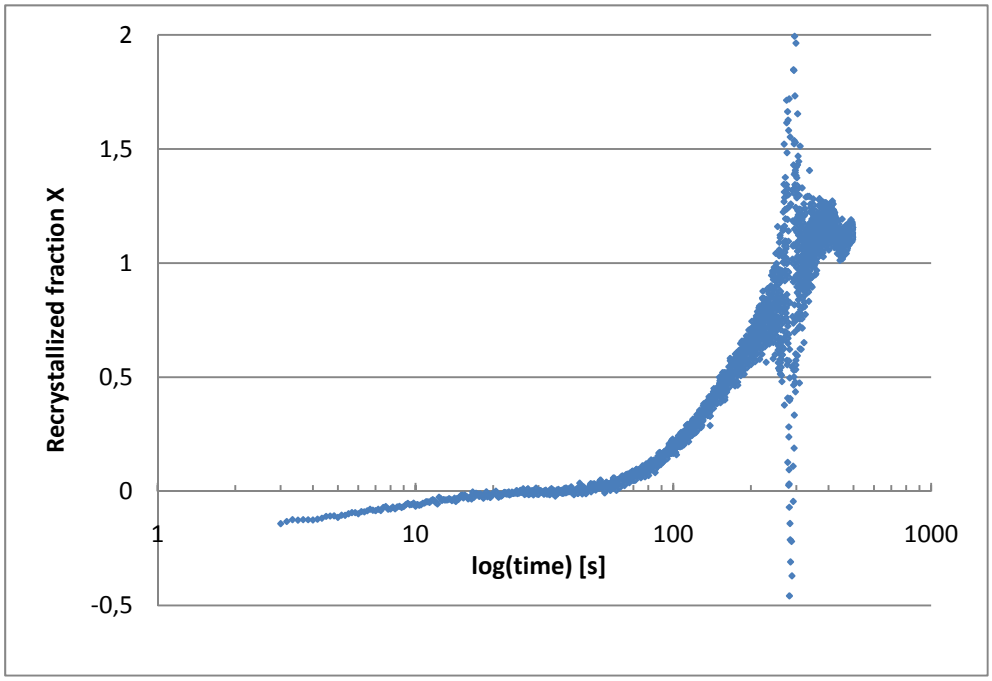

Fig. 5.27. Recrystallized fraction: stress relaxation sample (950°C, $0.1s^{-1}$, 0.2, 500s relaxation)

The curve representing recrystallized fraction vs. log(time) has a sigmoidal shape as expected. The recrystallization seems to start after 40s relaxation and is completed after 246s relaxation. These values coincide with the observations done on the pictures obtained with optical microscope. We can deduce from this previous study that recrystallized fraction can be calculated from stress relaxation tests, as long as the hypotheses of the model represent 0% and 100% recrystallization.

It had been reported in the bibliography that the strain, the strain rate and the temperature accelerate recrystallization when they are increased. From this knowledge and taking into account the results of the technique calibration, some assumptions can be done for further exploitation of the results:

- At temperatures lower than 950°C, with the same strain of 0.2 and strain rate of 0.1s $^{-1}$, recrystallization is not complete.
- At 1000°C and 1050°C, it is assumed that full recrystallization is occurring.
- The recrystallization kinetics should be greater for higher temperatures if the other parameters are kept constant.
- The recrystallization kinetics should be greater for higher strain rates if the other parameters are kept constant.
- The recrystallization kinetics should be greater for higher strain if the other parameters are kept constant.

5.3.3.2. Experimental parameters influence on recrystallization kinetics

Now that the working area has been defined, the method can be applied to determine the recrystallized fraction and see the influence of the strain, the strain rate and the temperature on recrystallization kinetics.

Relaxation curves obtained at 900°C

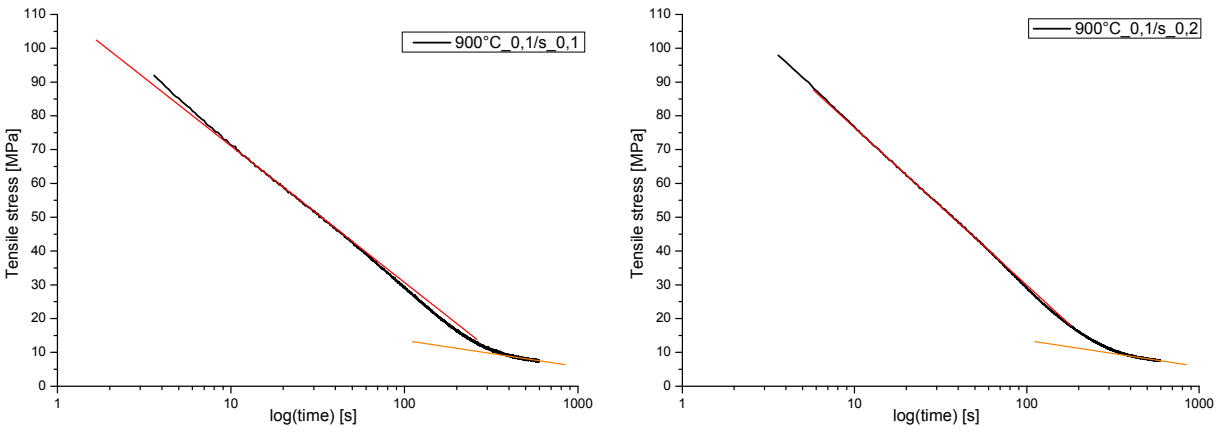

(a) (b)

Fig. 5.28. Stress relaxation curve: 900°C, strain rate of 0.1s-1 and (a) 0.1 strain; (b) 0.2 strain

Stress relaxation at 900°C for the 20%Mn TWIP steel (Fig. 5.28) does not show the typical changes in the slopes which indicate the beginning and the end of recrystallization. This could be caused because recrystallization is not occurring inside the material or the phenomenon is so small that it can't be detected by this method. Therefore, the recrystallized fraction cannot be extracted from these tests.

Influence of strain on recrystallization

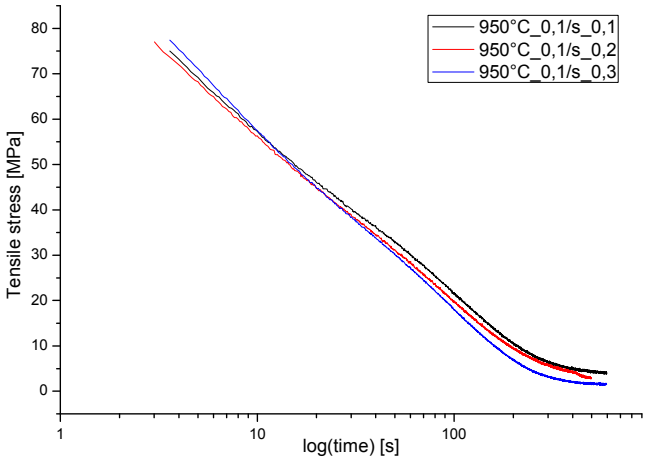

Fig. 5.29. Effect of strain on stress relaxation kinetics at 950°C for a 20%Mn TWIP steel

At 950°C, recrystallization kinetics is increased when the strain increased from 0.1 to 0.2 but from 0.2 to 0.3 there is no further influence since the two curves are almost superimposed (Fig. 5.30). The difference is even more difficult to perceive when dealing with stress relaxation curves (Fig. 5.29).

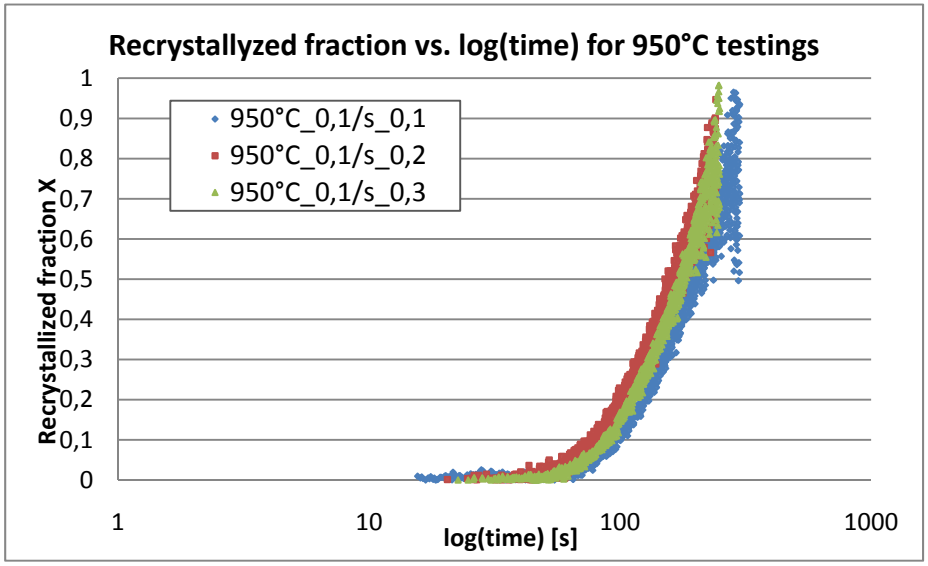

Fig. 5.30. Effect of strain on the recrystallization at 950°C for a 20%Mn TWIP steel

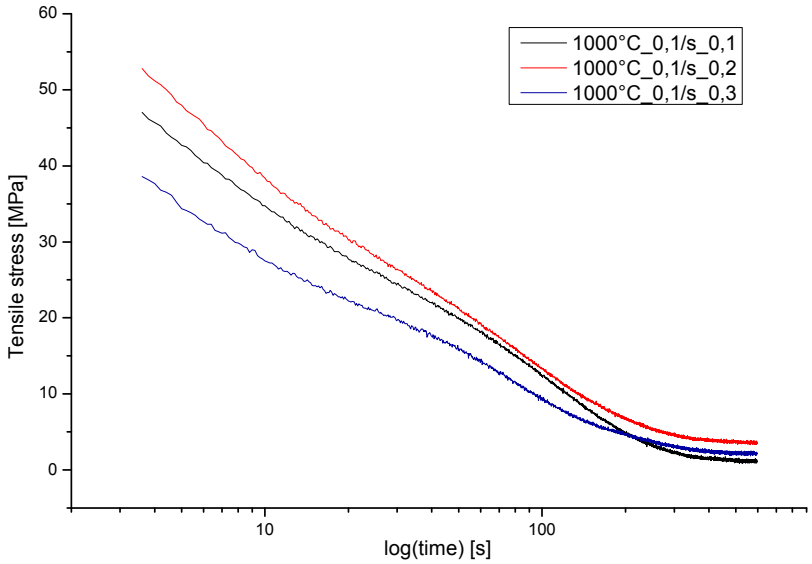

Fig. 5.31. Effect of strain on stress relaxation kinetics at 1000°C for a 20%Mn TWIP steel

The effect of strain seems to be more important when testing at 1000°C than at 950°C (Fig. 5.31).

Recrystallized fraction could be calculated because it could be assumed that recrystallization was complete. This assumption was made because at 950°C a fully recrystallized microstructure was obtained, therefore, at a higher temperature, recrystallization should also be complete after the same or shorter times because the system is supplied with more energy. Strain effect at 1000°C (Fig. 5.32) is similar to the effect at 950°C (Fig. 5.30). From 0.1 to 0.2 the recrystallization kinetics is increased since the slope of the curve is bigger but then, from 0.2 strain, any further increase does not make a significant difference.

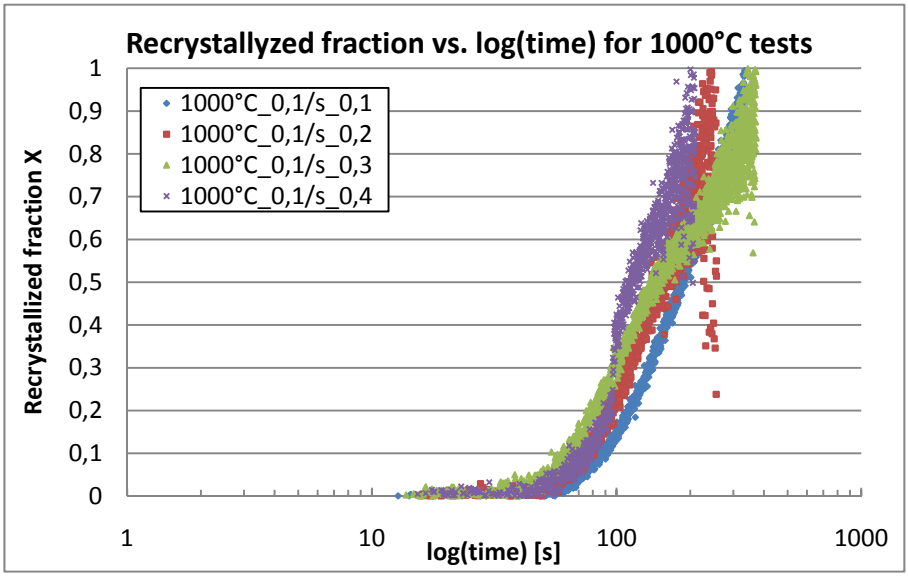

Fig. 5.32. Effect of strain on the recrystallization kinetics at 1000°C for a 20%Mn TWIP steel

In general, for a 20%Mn TWIP steel, strain has little influence on stress relaxation and on recrystallization kinetics, except for very small strains.

Influence of strain rate on recrystallization

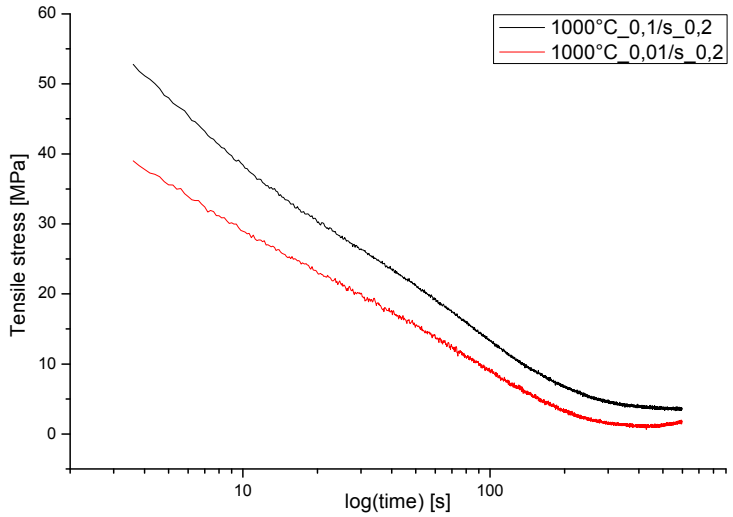

Fig. 5.33. Effect of strain rate on the recrystallization at 1000°C for a 20%Mn TWIP steel

The effect of strain rate has been tested at 1000°C (Fig. 5.33). A higher strain rate increases the recrystallization kinetics (Fig. 5.34). Nevertheless the effect of strain rate is of a great importance on recrystallization kinetics.

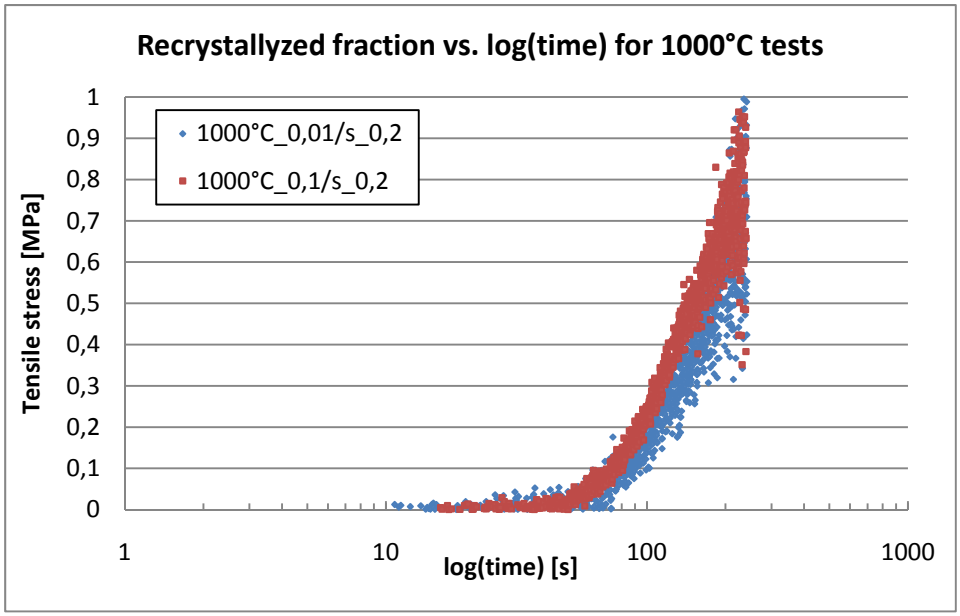

Fig. 5.34. Effect of strain rate on the recrystallization at 1000°C for a 20%Mn TWIP steel

Effects of temperature on recrystallization kinetics

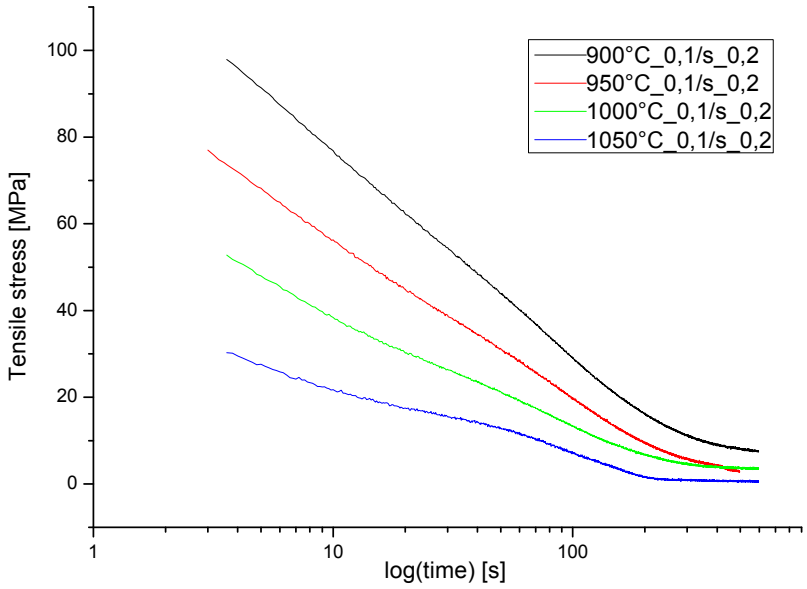

Fig. 5.35. Effect of temperature on the stress relaxation curves for a 20%Mn TWIP steel (strain rate $0.1s^{-1}$, strain: 0.2)

The increase in temperature is logically traduced by a softening of the material and consequently the lower the stress levels are the higher the temperature is (Fig. 5.35).

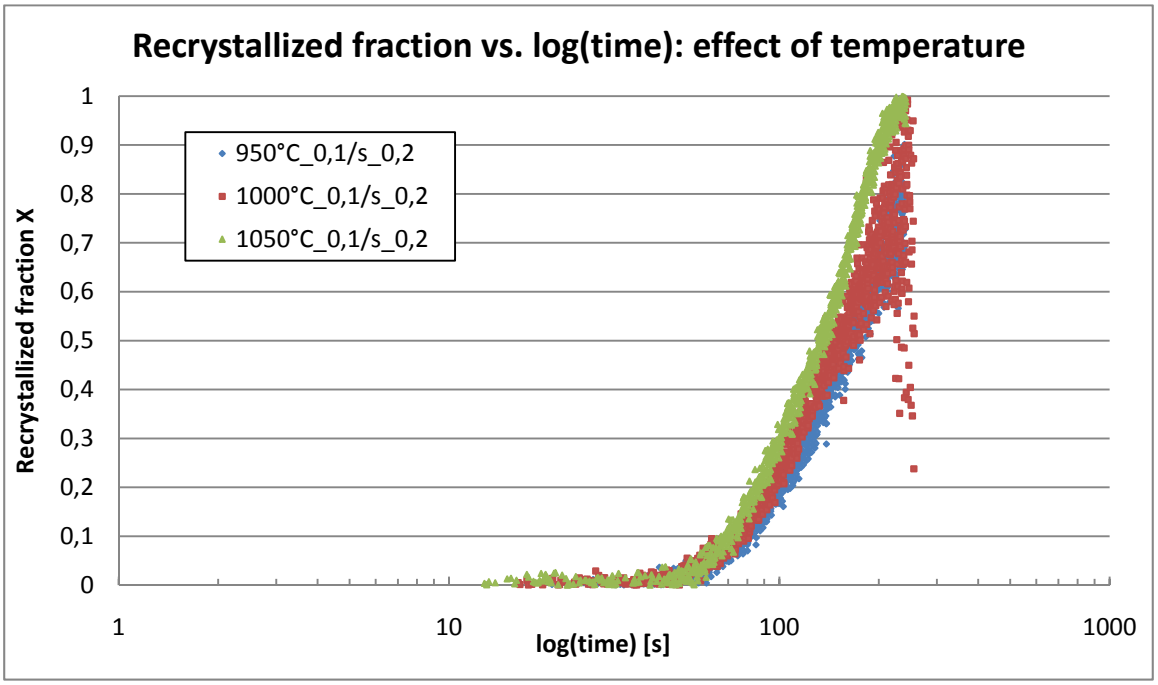

Fig. 5.36. Effect of temperature on the recrystallization kinetics for a 20%Mn TWIP steel (strain rate $0.1s^{-1}$, strain: 0.2)

When the recrystallized fraction is plotted for different temperatures (Fig 5.36), it can be observed that recrystallization kinetics is a bit increased when the temperature is increased.

5.3.3.3. Discussion and perspectives for stress relaxation tests

Discussion

As it can be seen on the relaxation curves (see, Fig. 5.31, 5.33 and 5.35), 20%Mn steel shows slight changes in the slopes of the curves when recrystallization takes place, even at elevated times. In comparison with the stress relaxation curves reported in the literature for other materials, recrystallization for the TWIP steel does not show a pronounced softening effect.

This behavior can be related to the material itself, that is to say TWIP steels are very little subjected to stress relaxation when recrystallizing. In other words, the recrystallized microstructure with a fine grain size is not much softer than the deformed microstructure. Another possibility would be that strengthening mechanisms could be interfering with recrystallization and the addition of both mechanisms promotes relaxation curves with no evident changes in slopes. Precipitation or phase transformation would be likely strengthening mechanisms. However, some thermodynamic calculations carried out with the software FactSage (Fig. 5.37) show that these phenomena are not expected to be taking place in the 20%Mn TWIP steel. The liquid phase is fully replaced by austenitic solid phase at 1300°C and a small cementite phase is created below 700°C. Yet, the characteristics of stress relaxation curves for the 20%Mn steel are inherent of the chemical composition and the experimental conditions, i.e., when recrystallization is eased by increasing the temperature, the softening related to recrystallization becomes more evident and promotes pronounced changes in the slopes of relaxation curves.

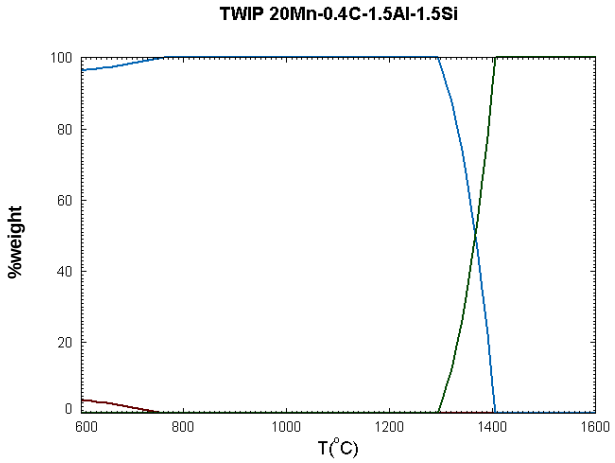

Fig. 5.37. Phase transformation diagram for a 20%Mn TWIP steel

Grain size originated during the heat treatments might be another parameter to take into account. For the 20%Mn TWIP steel, reheating at 1200°C promotes a grain size which might be too large to enable the recrystallization to occur extensively inside the material. Grain boundaries are preferential sites for recrystallization to occur which means that less energy is necessary for the nucleation and the growth of new grains. Intragranular nucleation is also possible but more energy has to be furnished to promote the growth of new grains. In fact it can be seen in Fig. 5.21 that recrystallization starts at grain boundaries and only after long recrystallization times the new grains form extensively in the whole microstructure. It is considered that the coarse grains generated during the heat treatment might be the cause of bigger recrystallization times obtained in this work when compared with the results in the literature [L. P. KARJALAINEN et al. 1996].

For the curves which do not exhibit the two changes of slopes, but just one after long relaxation times (see Fig. 5.28), it is assumed that relaxation might have started but not finished. This behavior is promoted by low temperatures and small strains. When this behavior was obtained, it was not possible to calculate recrystallization fractions. Analytically, when recrystallization was not finished, the asymptotes (red and blue) (see Fig. 5.38) happened to cross in the middle of the relaxation portion of the curve. This phenomenon directly influences the model used to calculate the recrystallized fraction. The intersection of the asymptotes represents the unique value that cancels the denominator of the equation that gives the recrystallized fraction.

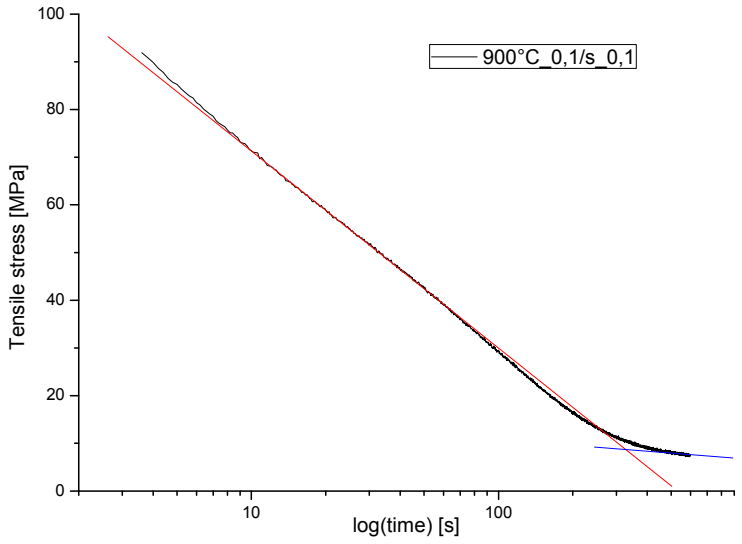

Fig. 5.38. Stress relaxation test for a 20%Mn TWIP steel (temperature: 950°C, strain rate: $0.1s^{-1}$, strain: 0.2)

Demonstration

The point where the two asymptotes cross is verifying the following equation (Eq. 5.1):

$$\sigma_1 - \alpha_1 \log t = \sigma_2 - \alpha_2 \log t \quad (5.1)$$

This equation can be written:

$$(\sigma_1 - \sigma_2) - (\alpha_1 - \alpha_2) \log t = 0 \quad (5.2)$$

This equation (Eq. 5.3) corresponds to the denominator of χ, the recrystallized fraction.

$$\chi = \frac{(\sigma_1 - \alpha_1 \log t) - \sigma}{(\sigma_1 - \sigma_2) - (\alpha_1 - \alpha_2) \log t} \quad (5.3)$$

Therefore χ can't be calculated if the asymptotes happen to cross when stress relaxation is occurring.

The model described by Karjalainen [L.P. KARJALAINEN, 1995], already considered that the method as-described in the section 3.2.3.2 can only be applied if recrystallization is complete. If no full recrystallization has taken place, the model is no longer adapted because the third stage of the relaxating curve is supposed to be the fully softened state. In the same paper, the authors presented a method which would be suitable when recrystallization was not full. For these conditions, the baseline for the fully recrystallized state should be calculated with an additional relaxation test carried out after applying a very small deformation. Unfortunately, this test was not done in this project.

Future work

The future work will include the determination of recrystallization kinetics for the 18%Mn and 25%Mn TWIP steels. The results will be useful to evaluate the effect of the composition on softening behavior at high temperature of TWIP steels. Moreover, the effect of initial grain size on stress relaxation curves will be analyzed because the heat treatments applied to these steels generated a homogeneous microstructure which was much finer than the one obtained for the steel with 20%Mn reported in this work.

The future work will include as well the realization of stress relaxation tests at very small strain, for instance 0.02. This test would provide a baseline for the other tests and could be used to calculate partial recrystallized fraction, as it is mentioned in Karjalainen article [L.P. KARJALAINEN, 1995].

Conclusions

Metallographies taken from 20%Mn TWIP steel samples which had been subjected to tensile tests showed that twinning is the main deformation mode and it takes place since the early stages of the deformation, i.e. after 0.3 deformation extensive twinning was already identified in the microstructure.

For the 18%Mn and the 25%Mn TWIP steel it was considered that the optimal heat treatment was at 1100°C for an hour. For the 20%Mn TWIP steel, the optimal heat treatment is at 1200°C for an hour. These treatments are performed at sufficient temperature to generate a new homogenous microstructure free of stresses limiting at the same time an excessive grain growth. A comparison of 18%Mn and 25%Mn steels indicate an effect of Mn on retarding the grain growth.

Stress relaxation tests demonstrated that static recrystallization occurs in 20%Mn TWIP steel at temperatures between 950°C and 1050°C. It was proved by metallographic evaluations. Moreover, it was observed that static recrystallization could be detected by this stress relaxation method in conditions that promote an eased recrystallization in the steel, i.e. at elevated temperatures.

The recrystallized fraction was calculated from these stress relaxation tests and these results provided important information about recrystallization kinetics and the influence of experimental parameters.

At 950°C and 1000°C, when the strain increases, the recrystallization kinetics is a bit faster. Though, this phenomenon is more visible at higher temperatures. The effect of strain rate on recrystallization kinetics is not really detectable at 1000°C, though it seems that increasing the strain rate accelerates the recrystallization kinetics. The effect of temperature is the most important on recrystallization kinetics, which increases when the temperature is raised.

It was observed that stress relaxation tests save a lot of time and material in comparison with double-hit tests. The recrystallization kinetics is obtained with a single test whereas several tests are necessary with the double-hit method to draw a single curve of recrystallized fraction as a function of time.

Further stress relaxation tests should be performed on the 18%Mn and 25%mn TWIP steels to evaluate the effects of composition and initial grain size on softening behavior of TWIP steels.

Acknowledgments

This work has been carried out in the Universitat Politècnica de Catalunya (UPC) in the Escola Tècnica Superior d'Enginyeria Industrial de Barcelona (ETSEIB) between spetember 2010 and February 2011.

I would like to thank mi tutor the doctor Jessica Calvo for her scientific supervision, valuable knowledge, her constructive comments and her help during the realization and redaction of this project. I learn very much from her scientific expertise in the field of metallurgy.

Of course, this work would not have been possible without the help of a few other people. So I thank Ahmed Boulaajaj for teaching me metallurgic techniques and for his infinite patience. I'd like to thank Ana Hernández Expósito for realizing the compression tests in Manresa with me; for her valuable knowledge, in science and in Spanish, and for her patience with these capricious TWIP steels. And I thank Isaac López Insa for his help with microscopes.

Many thanks to all the people working in the Departament de Ciència dels Materials i Enginyeria Metal•lúrgica (CMEM) for their reception and help.

Finally I'd like to thank my friends Casi and Aurélie for their moral support in every moment of this project. They've always known how to cheer me up with their great sense of humor, and I'm very thankful for that.

Bibliography

S. ALLAIN, J.-P. CHATEAU, O. BOUAZIZ [et al.], *Correlations between the calculated stacking fault energy and the plasticity mechanisms in Fe–Mn–C alloys*, Materials Science and Engineering A 387–389 (2004) 158–162]

T. BAJOR [et al.], Archives of Materials Science and Engineering, Vol. 28, June 2007, p. 337-340

J. M. CABRERA MARRERO, Thesis: *Caracterización mecánico-metalúrgica de la conformación en caliente del acero microaleado de medio carbono 38MnSiVS5, 1995*.

CHARLES J, BERGHE'ZAN A & LUTTS A, *Structural and Mechanical Properties of High-Alloy Manganese-Aluminum Steels*. 1982, J Phys 43: C4-435

J.-L . COLLET, Thesis: *Les mécanismes de déformation d'un acier TWIP FeMnC : une étude par diffraction des rayons X*, 2009

A. DELON, Thesis: Caracterización *de la recristalización estática de un acero TWIP*, Feb. 2010

H. DING, *Microstructures and Mechanical Properties of Fe-Mn-(Al, Si) TRIP/TWIP Steels,* Journal of iron and steel research, international. 2006, 13(6), p. 66-70

R. D. DOHERTY [et al.], Materials Science and Engineering A, 238(1997), No. 2, 219-274.

A. DUMAY, J.-P. CHATEAU, S. ALLAIN, S. MIGOT, O. BOUAZIZ, *Influence of addition elements on the stacking-fault energy and mechanical properties of an austenitic Fe–Mn–C steel,* Materials Science and Engineering A 483–484 (2008) 184–187

P. FABRÈGUE, Métallurgie du laminage à chaud, Techniques de l'ingénieur, TI-m7860]

G. FROMMEYER, U. BRÜX AND P. NEUMANN, *Supra-Ductile and High-Strength Manganese-TRIP/TWIP Steels for High Energy Absorption Purposes*, ISIJ International, Vol. 43 (2003), No. 3, pp. 438–446

P. D. HODGSON, S. H. ZAHIRI and J. J. WHALE, *The Static and Metadynamic Recrystallization Behaviour of an X60 Nb Microalloyed Steel*, ISIJ International, Vol. 44 (2004), No. 7, pp. 1224–1229

I. KARAMAN [et al.], *The deformation of low stacking-fault energy austenitic steels,* JOM, July 2002, 54.7; ABI/INFORM Trade & Industry pg.31

L.P. KARJALAINEN, *Stress relaxation method for investigation of softening kinetics in hot deformed steels*, Materials Science and Technology, vol.11, June 1995, p. 557-565

L.P. KARJALAINEN and J.PERTTULA, *Characteristics of Static and Metadynamic Recrystallization and Strain Accumulation in Hot-deformed Austenite as Revealed by the Stress Relaxation Method*, ISIJ International, Vol. 36 (1996), No. 6, p. 729-736

J. G. LENARD, MACIEJ PIETRZYK, L. CSER, *Mathematical and physical simulation of the properties of hot rolled products*, 1999, p. 151-164

X. LIN LI and T. Y. HSU (XU ZUYAO) *Gibbs free energy evaluation of the FCC(γ) and the HCP(ε) phases in the Fe-Mn-Si alloys*, 1997, Calphad vol. 21, N°3, pp. 443-448.

L. LISSEL, Thesis: *Modeling the Microstructural Evolution during Hot Working of C-Mn and of Nb microalloyed Steels using a Physically Based Model*, September 2006

R. M. PINEDA HUITRÓN, Thesis: *Conformabilidad en caliente de aceros twip*, Dec. 2009

K.P. RAO, Y.K.D.V. PRASAD, E.B. HAWBOLT, *Study of fractional softening in multi-stage hot deformation,* Journal of Materials Processing Technology 77 (1998) 166–174

W.P. SUN, MILITZER M., HAWBOLT E. B. AND MEADOWCROFT T. R., *Austenite grain refinement and growth during the thermomechanical processing of steels*, Hot Workability of Steels and Light Alloys-Composites; Montreal, Quebec; Canada, 1996, 285-292. 26

WORLDAUTOSTEEL, *Advanced High strength steel (AHSS) Application guidelines*, version 4.1, 2009

Appendices

Costs evaluation

It has been supposed that the project was required by a company to study these steels in the university, and this work has been done by a qualified engineer.

Projects costs are due to two causes, on the one hand for the material used during this work and on the other hand for the investigation itself. Costs for the material include sample metallographic preparation, use of software, and documents printing. Investigation costs include the time spent to characterize the samples metallography, that is to say hours of microscope observations but also calculations and documentary work realized for the interpretation of the results. Compression tests were realized with the help of a qualified technician, who is paid 42€/hour.

Costs for the material

Material	Units	Price / unit [€/]	Total cost [€]
Compression samples manufactured by electrical discharge machining	60	50/sample	3000
Material for the metallographic preparation	-	-	150
Image analyzing and data computing software (computer equipments, licenses, etc.)	-	-	600
High compression tests	60	195/sample	11 700
Other, like material used for the sample preparation and characterization (laboratory and office supplies)	-	-	600
TOTAL			**16 050**

Investigation costs

Investigation	Units	Price / unit [€/]	Total cost [€]
Images analysis	50	40/sample	2 000
Hours for metallographic preparation and characterization	300	20	6 000
Qualified engineer fees	640	50	32 000
TOTAL			**40 000**

Environmental impact

Adequate measures were taken during this investigation project to pay attention to the environmental impact. The impact during the realization of this project and also the global impact of high manganese content austenitic steels were taken into account.

Environmental impacts while realizing this project.

A special attention has been carried during this project to the recycling of the wastes, a good utilization of toxic products, a energy save for each tests that were specifically designed for the benefit of the project without wasting energy and material.

Environmental impacts of TWIP steels

TWIP steels are specially designed to reduce environmental impact of automotive industries. The aim is to reduce the weight of each car in order to lower its fuel consumption and its CO_2 emissions. This goal can be achieved thanks to the very good properties of TWIP, a improved strength combined to a high ductility, that enables car designers to reduce the thickness of each piece while conserving, or even increasing, crash performances and safety on board.

TWIP steel pictures

Transverse cut metallographic evaluation pictures referred in the paragraph 5.3.3.1 are presented below, for a matter of size.

Observation in the longitudinal direction of the sample (stress relaxation at 950°C, strain rate of $0.1s^{-1}$, strain of 0.2 and relaxation for 50s)

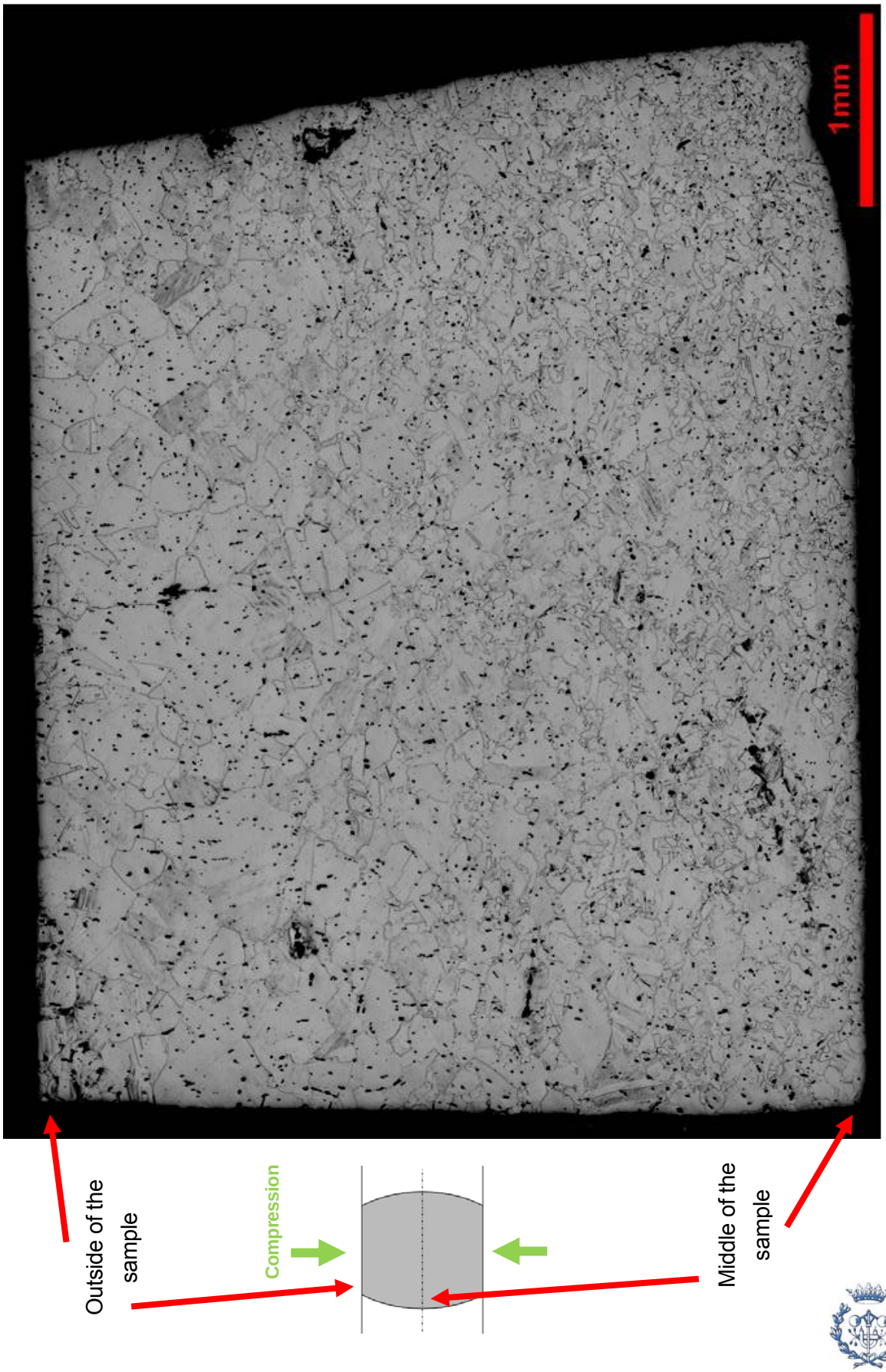

Observation in the longitudinal direction of the sample (stress relaxation at 950°C, strain rate of $0.1s^{-1}$, strain of 0.2 and relaxation for 100s)

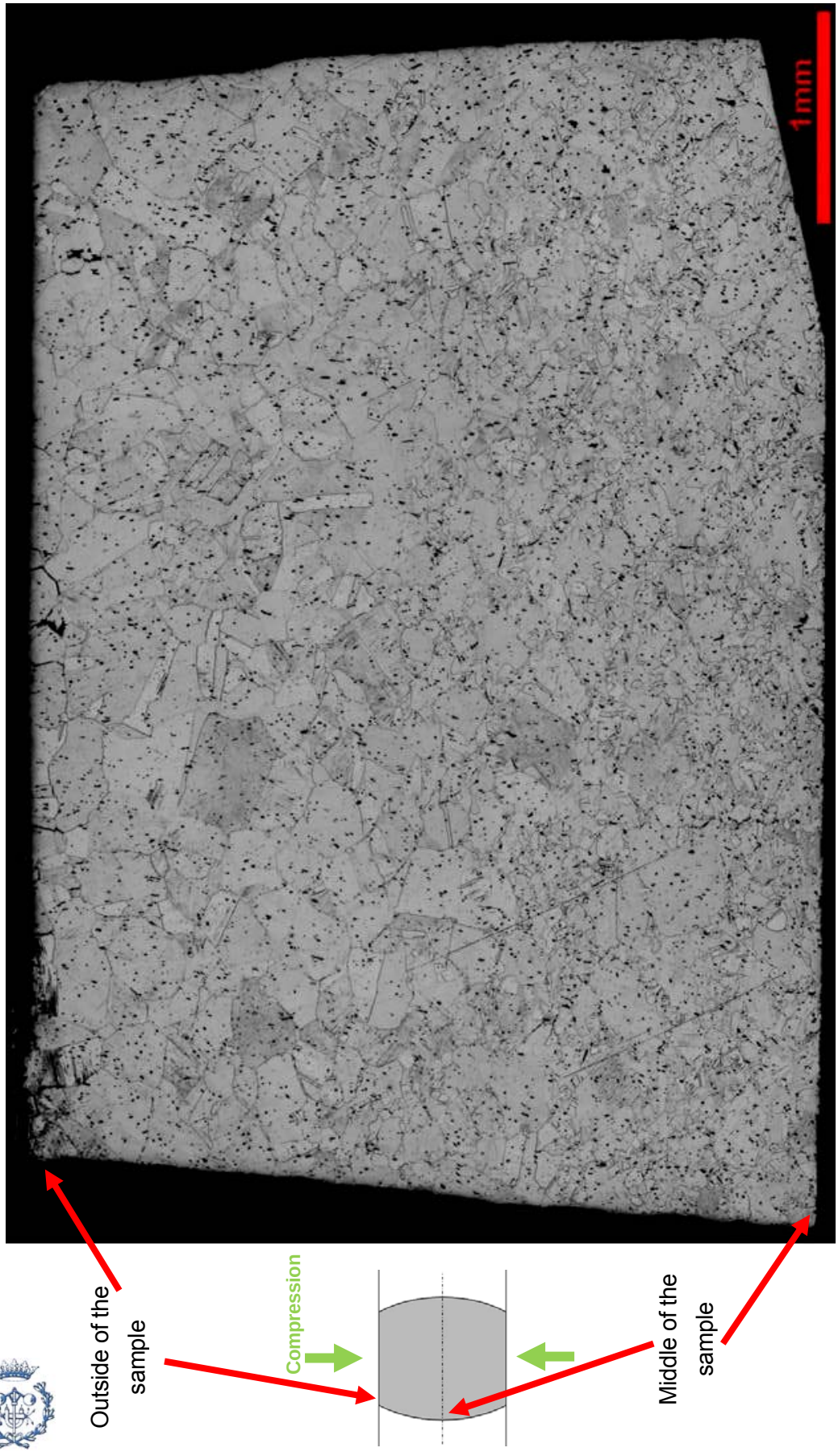

Observation in the longitudinal direction of the sample (stress relaxation at 950°C, strain rate of $0.1s^{-1}$, strain of 0.2 and relaxation for 200s)

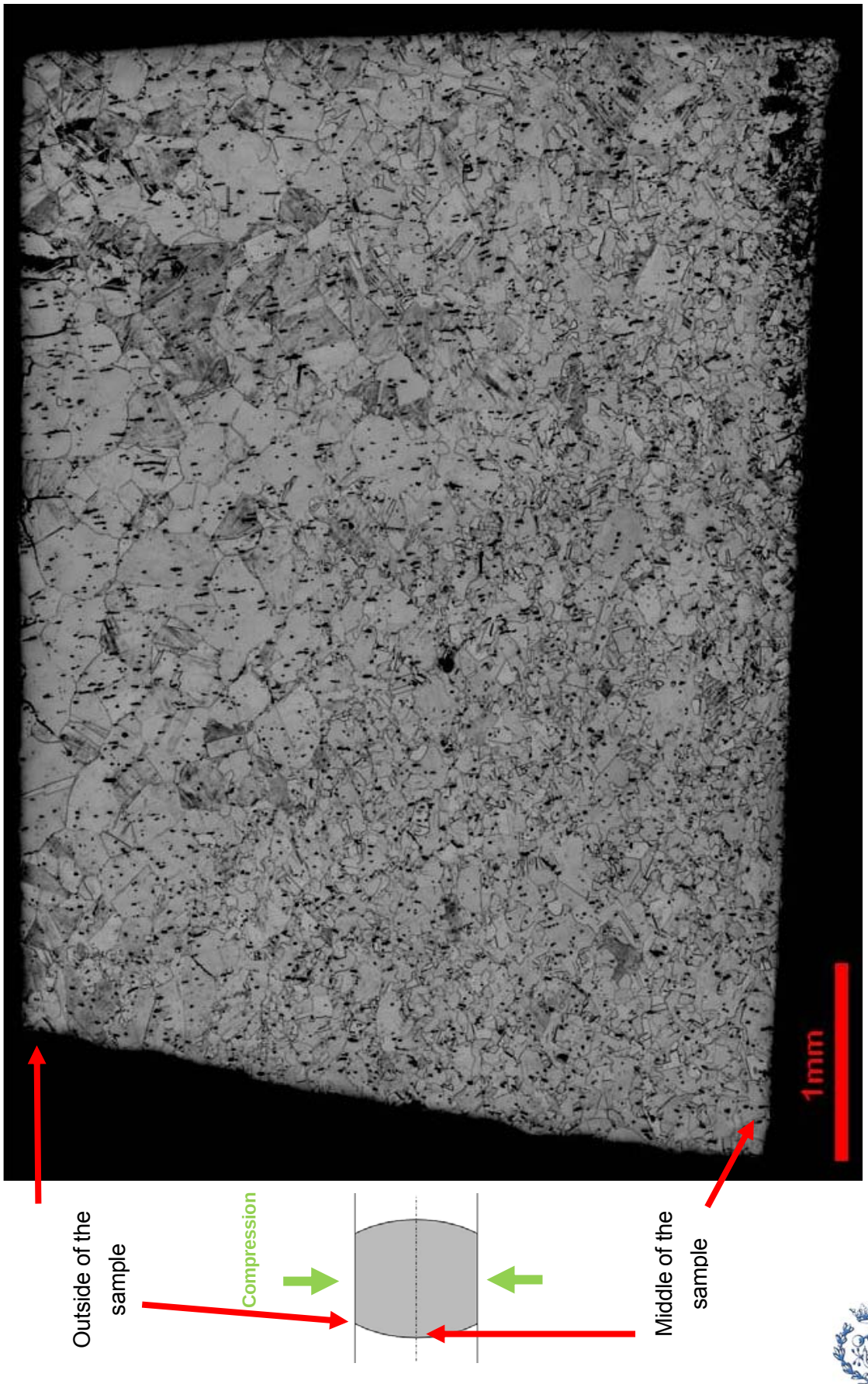

Observation in the longitudinal direction of the sample (stress relaxation at 950°C, strain rate of $0.1s^{-1}$, strain of 0.2 and relaxation for 500s)